

Copyright © 1996, by the author(s).
All rights reserved.

Permission to make digital or hard copies of all or part of this work for personal or classroom use is granted without fee provided that copies are not made or distributed for profit or commercial advantage and that copies bear this notice and the full citation on the first page. To copy otherwise, to republish, to post on servers or to redistribute to lists, requires prior specific permission.

**A SIMPLE TRANSFORMER MODEL APPLIED TO
A PLANAR INDUCTIVE PLASMA DISCHARGE**

by

J. T. Gudmundsson and M. A. Lieberman

Memorandum No. UCB/ERL M96/3

31 January 1996

**A SIMPLE TRANSFORMER MODEL APPLIED TO
A PLANAR INDUCTIVE PLASMA DISCHARGE**

by

J. T. Gudmundsson and M. A. Lieberman

Memorandum No. UCB/ERL M96/3

31 January 1996

ELECTRONICS RESEARCH LABORATORY

College of Engineering
University of California, Berkeley
94720

A Simple Transformer Model Applied to a Planar Inductive Plasma Discharge

J. T. Gudmundsson¹ and M.A. Lieberman²

¹Department of Nuclear Engineering,

²Department of Electrical Engineering and Computer Sciences,
University of California at Berkeley,
Berkeley, CA 94720

Abstract

A planar inductive radio frequency discharge is modeled as a transformer with the inductive coil taken as the primary circuit and the plasma as the secondary circuit. The mutual inductance between the primary and secondary circuit, the self inductance of the plasma and the impedance of the plasma are determined theoretically and related to the properties of the plasma. The model is applied to argon plasma in the pressure range 2 – 60 mTorr and electron densities in the range 10^{16} – 10^{20} m^{-3} . The model calculations are compared to measured impedance, rf current and rf voltage, showing good agreement.

1 Introduction

Inductively coupled rf discharges can provide high density plasma with low ion bombarding energy. In an inductive source the plasma is created by applying rf power to a non-resonant, inductive coil, resulting in the breakdown of the process gas within or near the coil by the induced electric field. As shown in figure 1 (a) low pressure inductive discharges have been studied by considering the plasma to be the secondary coil of an air-core transformer [1, 2, 3]. The primary inductive coil has inductance L_o and resistance R_o . The secondary discharge inductance can be considered to consist of two components, a geometric inductance and an inertia inductance. The electrical properties of the plasma are described by the plasma conductivity

$$\sigma_p = \frac{e^2 n_e / m}{\nu_{eff} + j\omega_{eff}} \quad (1)$$

where ν_{eff} is the effective collision frequency, n_e is the electron density and ω_{eff} is the effective driving frequency, where kinetic effects of electron collisions are taken into account [4]. The real part of the plasma conductivity defines the plasma resistance R_2 and the imaginary part defines the inductance L_e due to the electron inertia [2] which can be written as

$$L_e = \frac{R_2 \omega_{eff}}{\nu_{eff} \omega} \quad (2)$$

where ω is the driving frequency. ω_{eff} lies near ω and depends weakly on the pressure; ν_{eff} is approximately proportional to the pressure. Both ω_{eff} and ν_{eff} are defined in section 3.4 and are determined in section 6. The geometric inductance L_2 is due to a current path formed within the discharge. Seen in the primary circuit, as shown in figure 1 (b), the effect of the coupled secondary circuit is to add the impedance $Z_2(\omega M)^2/|Z_2|^2$ to the primary circuit, where

$$Z_2 = R_2 + j \left[\omega L_2 + \frac{\omega_{eff}}{\nu_{eff}} R_2 \right] \quad (3)$$

is the complex impedance of the secondary circuit and M is the mutual inductance between the the primary and secondary circuit. In this simple model the change in primary resistance due to plasma loading is

$$\rho = R_1 - R_o = \frac{\omega^2 M^2}{|Z_2|^2} R_2 \quad (4)$$

where R_1 is the total resistance seen in the primary circuit. The change in primary reactance is

$$\chi = \omega(L_1 - L_o) = \frac{\omega^2 M^2}{|Z_2|^2} \left[\omega L_2 + \frac{\omega_{eff}}{\nu_{eff}} R_2 \right] \quad (5)$$

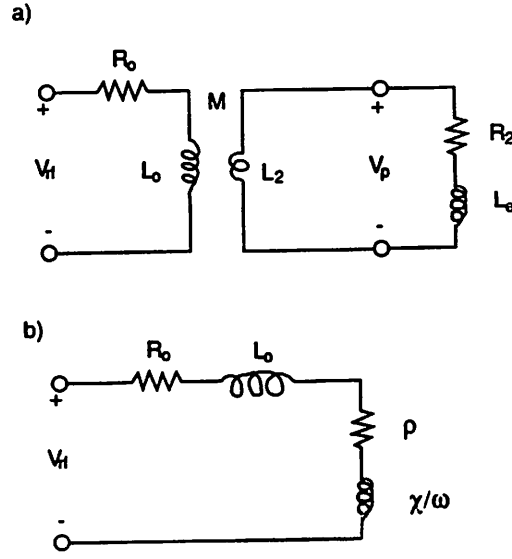


Figure 1: The transformer circuit. (a) The primary circuit has inductance L_0 and resistance R_0 and the secondary circuit consist of geometric inductance L_2 , electron inertia inductance L_e and the plasma resistance R_2 . (b) The secondary circuit transformed into the primary circuit. The change in primary circuit impedance due to plasma loading is $\rho + j\chi$.

where L_1 is the total inductance seen in the primary circuit. The power absorbed within the plasma is given by

$$P_{abs} = P_2 = \rho I_{rf}^2 \quad (6)$$

where I_{rf} is the rms current in the primary coil.

2 Experiment

The plasma is created inside a cylindrical vacuum chamber of radius $R = 15.24$ cm and length $L = 7.62$ cm. A 2.5 cm thick by 25 cm diameter quartz plate separates the planar spiral induction coil from the plasma (see figure 2). The primary coil is a three turn coil made of 0.06 cm thick and 1.9 cm wide copper strip with outer radius $a_o = 9.09$ cm and 3 cm spacing between turns. The coil is placed 0.3 cm away from the quartz plate. A Faraday (electrostatic) shield was not used in these experiments.

The source is powered at 13.56 MHz using a 1 kW Henry 1000D Radio Frequency Power Generator connected to an L-type capacitive matching network as seen in figure 3. The matching network consist of a shunt capacitor having a variable capacitance

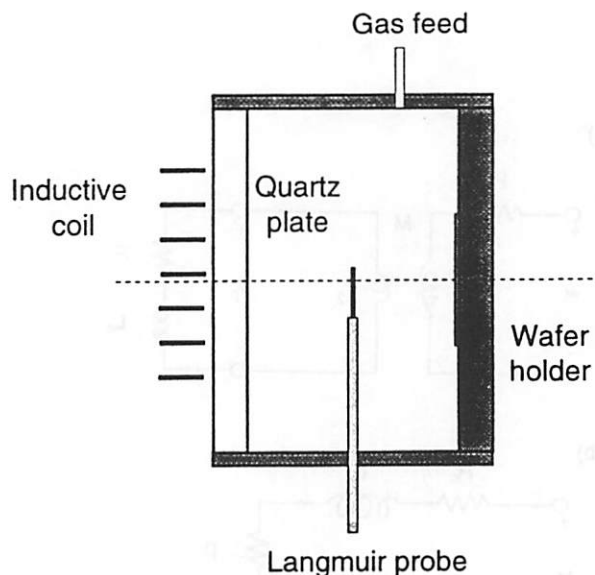


Figure 2: Cross section of the vacuum chamber. The primary coil is on the left hand side, next to the quartz window. The Langmuir probe is installed to measure the plasma parameters at the center of the chamber.

$C_2 = 750 - 1700$ pF and a series capacitor of variable capacitance $C_1 = 25 - 500$ pF. The variable capacitors can be adjusted to match the 50Ω output resistance of the power supply to the inductive coil.

2.1 Electrical Measurements

A Bird Electronics Model 43 watt meter, placed between the generator and the matching network measures the power flow to the discharge P_{inc} and the reflected power P_{rfl} . The power transmitted to the circuit is the difference $P_{tr} = P_{inc} - P_{rfl}$. The power absorbed within the plasma is determined by measuring the power absorbed when plasma is present in the source and the current applied. These values give the resistance R_1 . Similarly the power and the current are measured when no plasma is present to give the resistance of the primary coil R_o . By subtracting R_o from R_1 and multiplying by the square of the applied current, the power absorbed in the plasma is found. The current is measured using a Pearson Model 411 current monitor at the low voltage terminal of the coil, as seen in figure 3. The coil voltage is measured using a capacitive voltage divider.

3 Transformer Model

A transformer consists of two windings interlinked by a mutual magnetic field. The magnetic field produced by a current flowing in the primary coil interacts with the

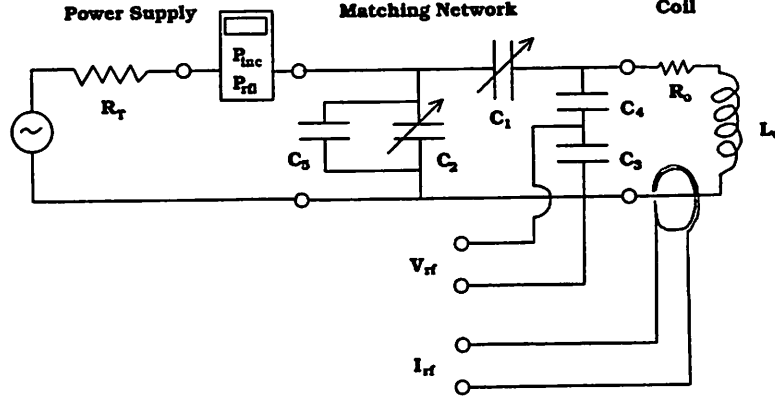


Figure 3: The circuit diagram showing the power supply, matching network and the inductive coil. The power meter shows the incident and reflected power. The current transformer has output I_{rf} and the voltage across the coil is measured using a capacitive voltage dividing.

secondary coil. An inductively coupled discharge consist of an induction coil (the primary coil) and the discharge which can be thought of as the secondary coil.

For static coupled circuits the inductances are constants and the inductance matrix is defined by (see figure 1 (a))

$$V_{rf} = j\omega L_o I_{rf} + j\omega M I_p + R_o I_{rf} \quad (7)$$

$$V_p = j\omega M I_{rf} + j\omega L_2 I_p \quad (8)$$

where L_o is the inductance of the primary coil, M is the mutual inductance between the coils and L_2 is the geometric (or magnetic) inductance of the plasma. Using $V_p = -I_p(R_2 + j\frac{\omega e f f}{\nu_{eff}} R_2)$ in equation (8) and inserting into equation (7) we can solve for the impedance seen at the primary coil terminals

$$Z_s = \frac{V_{rf}}{I_{rf}} = R_s + j\omega L_s \quad (9)$$

where

$$R_s = R_o + \frac{\omega^2 M^2 R_2}{R_2^2 + \left(\frac{\omega e f f}{\nu_{eff}} R_2 + \omega L_2\right)^2} \quad (10)$$

is the resistance and

$$L_s = L_o - \frac{M^2 \left(\frac{\omega e f f}{\nu_{eff}} R_2 + \omega L_2\right)}{R_2^2 + \left(\frac{\omega e f f}{\nu_{eff}} R_2 + \omega L_2\right)^2} \quad (11)$$

is the inductance. This yields the required rf source current and voltage for a given rf power P_{abs} absorbed by the plasma using $V_{rf} = I_{rf}Z_s$ and $P_{abs} = I_{rf}^2(R_s - R_o)$. This is discussed by Lieberman and Gottscho [5] for the cylindrical geometry. The various discharge parameters that go into equations (10) and (11) are modeled in the following sections for the planar coil geometry.

3.1 The Mutual Inductance

The mutual inductance between two circular loops is given by Maxwell [6] as

$$M = \mu_o \sqrt{ab} \left[\left(\frac{2}{\kappa} - \kappa \right) K(\kappa) - \frac{2}{\kappa} E(\kappa) \right] \quad (12)$$

where $K(\kappa)$ and $E(\kappa)$ are the complete elliptic integrals of the first and second kinds respectively. The parameter κ is defined by

$$\kappa^2 \equiv \frac{4ab}{d^2 + (a+b)^2} \quad (13)$$

and

$$\kappa'^2 \equiv \frac{(b-a)^2 + d^2}{(b+a)^2 + d^2} \quad (14)$$

where b is the mean radius of a plasma disk next to the dielectric window, $a = a_i$, $i = 0, 1, 2$ are the mean radii of each of the three turns of the inductive coil, and d is the distance between the center planes of the two circular loops. This distance is

$$d = \frac{\xi_1}{2} + \Delta + w_q + \frac{\delta}{2} \quad (15)$$

where ξ_1 is the width of the copper strip that forms the primary coil, Δ is the gap size between the primary coil and the quartz window, w_q is the quartz window thickness, and δ , the thickness of the plasma disk, is estimated to be the skin depth of the plasma. Note that

$$\kappa'^2 \equiv 1 - \kappa^2 \quad (16)$$

and all values of κ and κ' lie between zero and unity. Define as well

$$r_1^2 \equiv (b+a)^2 + d^2 \quad (17)$$

and

$$r_2^2 \equiv (b-a)^2 + d^2 \quad (18)$$

3.1.1 A Simple Approach

Consider current I' circulating in a circle of radius a . Then the magnetic field induced at an arbitrary position z along the axis is [7, p. 260]

$$B(z) = \frac{\mu_o I' a^2}{2(a^2 + z^2)^{3/2}} \quad (19)$$

The magnetic flux through an area, πb^2 , at distance $z = d$ from the circle is then

$$\varphi(d) = \frac{\mu_o I' \pi a^2 b^2}{2(a^2 + d^2)^{3/2}} \quad (20)$$

and the mutual inductance is thus

$$M = \frac{\varphi(d)}{I'} = \frac{\mu_o \pi a^2 b^2}{2(a^2 + d^2)^{3/2}} \quad (21)$$

which in the case of $b = \frac{1}{2}a_o$ and $a = a_i$ gives

$$M_i = \frac{\mu_o \pi a_i^2 a_o^2}{8(a_i^2 + d^2)^{3/2}} \quad (22)$$

Then the total mutual inductance due to the three turns of the coil is given by

$$M = \sum_{i=0}^{n=2} M_i \quad (23)$$

3.1.2 Coaxial Circular Coils

For a more accurate value of the mutual inductance the plasma is treated as a circular loop as well as each of the three turns of the primary coil. For each turn Maxwell's equation (12) in terms of κ' is used. Curtis and Sparks [8] recommend the use of

$$M_i = \frac{\mu_o r_{i1}}{4} \sum_{j=0}^{\infty} \frac{(2j)^2 \kappa'^{2j}}{2^{4j} (j^4)} \left[\frac{1}{(2j-1)} \ln \frac{16}{\kappa'^2} - \frac{4}{(2j-1)^2} + \frac{2\kappa'^2}{(j+1)(2j+1)} - \frac{\kappa'^2}{2(j+1)^2} \sum_{s=0}^j \frac{1}{(s+1)(2s+1)} \right] \quad (24)$$

for coaxial circular coils so arranged that $\kappa^2 > 0.4$.

3.1.3 Lyle's method

The value of the mutual inductance M calculated using the above methods is lower than the actual value, since the nearer portions of the coil contribute more to the

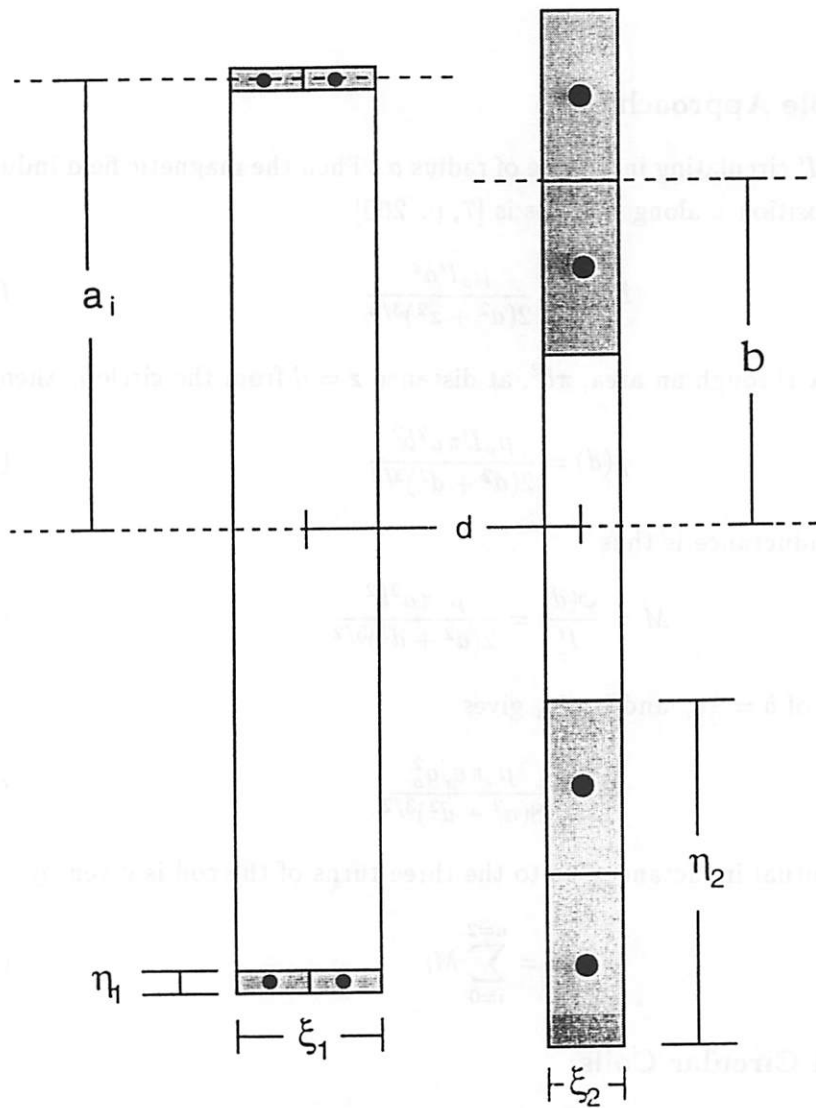


Figure 4: Lyles method, ξ_1 is the axial breadth and η_1 is the radial depth of the primary coil. The mean radii of each of the three turns of the coil is written a_i , $i = 0, 1, 2$, where 0 denotes the outermost coil. The conducting path within the plasma has axial breadth ξ_2 and radial depth η_2 .

Table 1: *The proper radii and separation to be used*

Mutual inductance	Proper radii	Plane distance
M_{13}	$\varrho_1, \varrho_2 + \zeta_2$	$d + \zeta_1$
M_{14}	$\varrho_1, \varrho_2 - \zeta_2$	$d + \zeta_1$
M_{23}	$\varrho_1, \varrho_2 + \zeta_2$	$d - \zeta_1$
M_{24}	$\varrho_1, \varrho_2 - \zeta_2$	$d - \zeta_1$

total mutual inductance than is compensated for by the smaller contributions farther away. A more accurate value is obtained by the use of Lyle's method [9, 10]. Each coil is split up into two equivalent filaments with half the current flowing in each.

Write ξ_1 as the axial breadth and η_1 as the radial depth of the inductive coil. The mean radii of each of the three turns of the coil is written a_i , $i = 0, 1, 2$, where 0 denotes the outermost coil. Similarly the coil formed by the plasma has axial breadth ξ_2 and radial depth η_2 (see figure 4 (after [10])).

The primary coil is such that $\xi_1 > \eta_1$ so the filaments have an equivalent radius slightly larger than the mean radii a_i defined by

$$\varrho_{1i} = a_i \left(1 + \frac{1}{24} \frac{\eta_{1i}^2}{a_i^2} \right) \quad (25)$$

and are located at an axial distance ζ_1 on either side of the median plane

$$\zeta_1^2 = \frac{\xi_1^2 - \eta_1^2}{12} \quad (26)$$

where $2\zeta_1$ is the equivalent breadth. The plasma is assumed to have a disk shape with mean radius, $b = \frac{1}{2}a_o$, axial breadth $\xi_2 = \delta$ and radial depth $\eta_2 = \frac{3}{4}a_o$, where δ is the skin depth of the plasma and a_o the radius of the inductive coil. Since $\frac{3}{4}a_o > \delta$, the radii of the two equivalent filaments become $\varrho_2 + \zeta_2$ and $\varrho_2 - \zeta_2$ respectively, where

$$\varrho_2 = b \left(1 + \frac{1}{24} \frac{\eta_2^2}{b^2} \right) \quad (27)$$

and the equivalent depth $2\zeta_2$ is defined by

$$\zeta_2^2 = \frac{\eta_2^2 - \xi_2^2}{12} \quad (28)$$

The mutual inductance for each of the three coils is then obtained using the proper radii and distances as shown in table 1 in equation (24). The average value of the four cases is found as

$$M_i = \frac{M_{i13} + M_{i14} + M_{i23} + M_{i24}}{4} \quad (29)$$

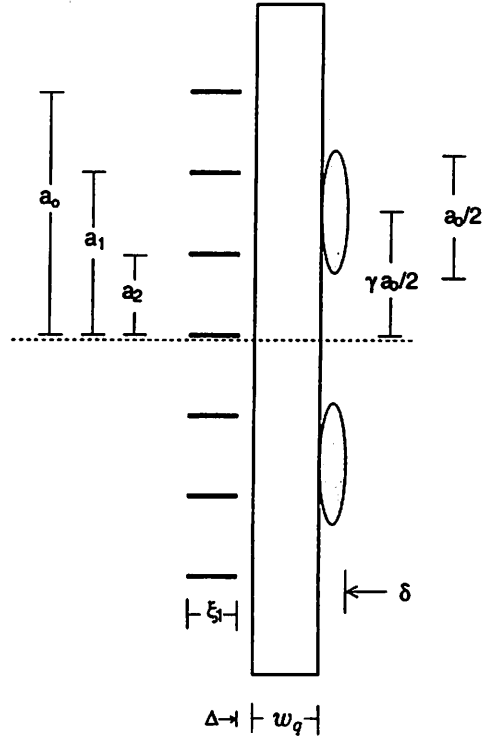


Figure 5: Cross section showing the primary coil, quartz plate and the conducting current path within the plasma.

and the total mutual inductance is calculated by using equation (23).

3.2 Self Inductance of Plasma Loop

In order to determine the self inductance of the plasma in the discharge it is assumed that a circular current path with an elliptically shaped cross section is formed next to the quartz window. The axial thickness of this current path is assumed to be equal to the skin depth of the plasma δ , which is the characteristic scale length of the induced rf current density in the power absorption region as seen in figure 5. Measurements using a magnetic induction probe have been used to determine the electric field distribution (proportional to the current density distribution) next to the dielectric window [11, 12]. Meyer and Wendt [12] measure the peak electric field to be located at about $\frac{3}{4}$ the outside radius of the inductive coil at 5 mTorr and at about $\frac{7}{8}$ the radius at 50 mTorr. To account for this expansion of the radial location of the maximum electric field with pressure we introduce a parameter γ . This parameter is estimated by linearly interpolating the position of the electric field peak with pressure from these data. γ 's for a few different values of pressure are listed in table 2. The electric field falls to half the peak value at about $\frac{1}{4}$ the coil radius toward each side.

The plasma is thus assumed to form a conducting loop of major radius, γa_0 , having an elliptically shaped cross section with minor radii $\frac{1}{4}a_0$ and $\frac{1}{2}\delta$, where δ is

Table 2: The loop expansion parameter γ

Pressure [mTorr]	γ
2	0.74
5	0.75
10	0.76
20	0.79
60	0.90

the skin depth of the plasma, and a_o is the radius of the outermost coil segment. The average radius of the plasma cross section is thus $\sqrt{\frac{1}{8}\delta a_o}$. The contribution to the inductance from external flux due to the mutual inductance between two concentric circles of radii γa_o and $\gamma a_o - \sqrt{\frac{1}{8}\delta a_o}$ is calculated using equation (24) where

$$\kappa'^2 = \frac{a_o \ell}{8(2\gamma a_o - \sqrt{\frac{1}{8}\delta a_o})^2} \quad (30)$$

and $r_1 = (2\gamma a_o - \sqrt{\frac{1}{8}\delta a_o})$, so that

$$L_2 = \mu_o \left(2\gamma a_o - \sqrt{\frac{1}{8}\delta a_o} \right) \sum_{j=0}^{\infty} \frac{(2j)^2 \kappa'^{2j}}{2^{4j} (j^4)} \left[\frac{1}{(2j-1)} \ln \frac{16}{\kappa'^2} - \frac{4}{(2j-1)^2} + \frac{2\kappa'^2}{(j+1)(2j+1)} - \frac{\kappa'^2}{2(j+1)^2} \sum_{s=0}^j \frac{1}{(s+1)(2s+1)} \right] \quad (31)$$

If $\kappa \approx 1$, equation (31) can be approximated by [13]

$$L_2 \approx \mathcal{R} \mu_o \left[\ln \left(\frac{8\mathcal{R}}{\bar{r}} \right) - 2 \right] \quad (32)$$

for a circular loop of major radius \mathcal{R} and minor radius \bar{r} . Using $\mathcal{R} = \gamma a_o$ and the mean radius $\bar{r} = \sqrt{\frac{1}{8}\delta a_o}$ gives

$$L_2 \approx \gamma a_o \mu_o \left[\ln \left(\frac{8\gamma a_o}{\sqrt{\frac{1}{8}\delta a_o}} \right) - 2 \right] \quad (33)$$

3.3 Plasma Resistance

The power dissipated within the plasma is given by

$$P_{abs} = 2\pi \int_0^{\infty} dz \int_0^R r dr \frac{J_{\theta}^2(r, z)}{\sigma_{dc}} \quad (34)$$

where J_θ is the rms current density, σ_{dc} is the electrical conductivity of the plasma and R is the radius of the chamber. The current profile is assumed to follow [14]

$$J_\theta(r, z) = J_{\theta_0} J_1(\gamma_1 r) \exp(-z/\delta) \quad (35)$$

where J_{θ_0} is the rms current density, $J_1(\gamma_1 r)$ is the first-order Bessel function and $\gamma_1 R = 3.83$. Integrating gives

$$P_{abs} = \frac{\pi J_{\theta_0}^2 \delta R^2}{\sigma_{dc}} \{J_0(\gamma_1 R)\}^2 \quad (36)$$

where $J_0(\gamma_1 r)$ is the zero-order Bessel function. The rms current flowing through the current path is found by integrating the current density over the cross section of this current path or

$$I_\theta = \int_0^\infty dz \int_0^R dr J_\theta(r, z) = \frac{J_{\theta_0} \delta}{\sqrt{2} \gamma_1} \{1 - J_0(\gamma_1 R)\} \quad (37)$$

The resistance of the plasma is then given using $P_{abs} = R_2 I_\theta^2$ as

$$R_2 = \frac{2\pi(\gamma_1 R)^2}{\sigma_{dc} \delta} \frac{\{J_0(\gamma_1 R)\}^2}{\{1 - J_0(\gamma_1 R)\}^2} \quad (38)$$

For $\sigma_{dc} = e^2 n_e / m \nu_{eff}$ we get

$$R_2 = 7.595 \frac{m \nu_{eff}}{e^2 n_e \delta} \quad (39)$$

Seen in the primary circuit, the plasma resistance is given by equation (4)

$$\rho = \frac{\omega^2 M^2 R_2}{R_2^2 + \left(\frac{\omega_{eff}}{\nu_{eff}} R_2 + \omega L_2\right)^2} \quad (40)$$

3.4 Effective Collision Frequency

The effective electron collision frequency consists of the electron neutral collision frequency and the stochastic collision frequency. In high density plasma the electron-ion collision frequency has to be added as well. The effective electron collision frequency is thus the sum

$$\nu_{eff} = \nu_{en} + \nu_{st} + \nu_{ei} \quad (41)$$

and approaches the electron neutral collision frequency in the high-pressure collisional limit. The relative importance of each of the collisional mechanisms depends on the gas type, neutral gas pressure and temperature, electron density of the plasma and the electron temperature.

3.4.1 Electron-Neutral Interaction

The electron neutral collision frequency depends on the neutral gas pressure and gas temperature and is usually given as

$$\nu_{en}^{(o)} = K_{el} n_g \quad (42)$$

where K_{el} is the rate coefficient for elastic scattering against neutral atoms and is given in figure 6 versus electron temperature for argon. Assuming the gas to be ideal

$$p = n_g k T_g \quad (43)$$

where p is the gas pressure, n_g is the neutral gas density, and T_g is the gas temperature, equation (42) becomes

$$\nu_{en}^{(o)} = \frac{p K_{el}}{k T_g} \quad (44)$$

In the limited range of interest for discharge operation, $1 \text{ V} \leq T_e \leq 7 \text{ V}$, the momentum transfer rate constant K_{el} can be approximated by

$$K_{el} \approx (3.45 T_e - 1.19) \times 10^{-14} \quad \text{m}^3/\text{s} \quad (45)$$

so given the gas temperature and the electron temperature the electron neutral collision frequency can be estimated.

Actually, equation (42) is strictly valid only for the calculation of the electron-neutral collision frequency $\nu_{en}^{(o)}$ if the collision cross section is independent of the electron energy. The general formula for the electron-neutral collision frequency and the effective driving frequency is [4]

$$\nu_{en} + j\omega_{eff} = -\frac{3}{2} \left[\int_0^\infty \frac{\mathcal{E}^{3/2}}{\nu_c(\mathcal{E}) + j\omega} \frac{df}{d\mathcal{E}} d\mathcal{E} \right]^{-1} \quad (46)$$

where $f(\mathcal{E})$ is the electron energy distribution function and

$$\nu_c = n_g \sigma_c(\mathcal{E}) \left(\frac{2e\mathcal{E}}{m} \right)^{1/2} \quad (47)$$

where $\sigma_c(\mathcal{E})$ is the collision cross section. The collision cross section for argon is given in figure 7 (compiled by Lister et al. [4]). ν_{en} and ω_{eff} depend on T_e , which will be evaluated from the discharge particle balance, equation (78), in section 6, assuming a Maxwellian electron energy distribution.

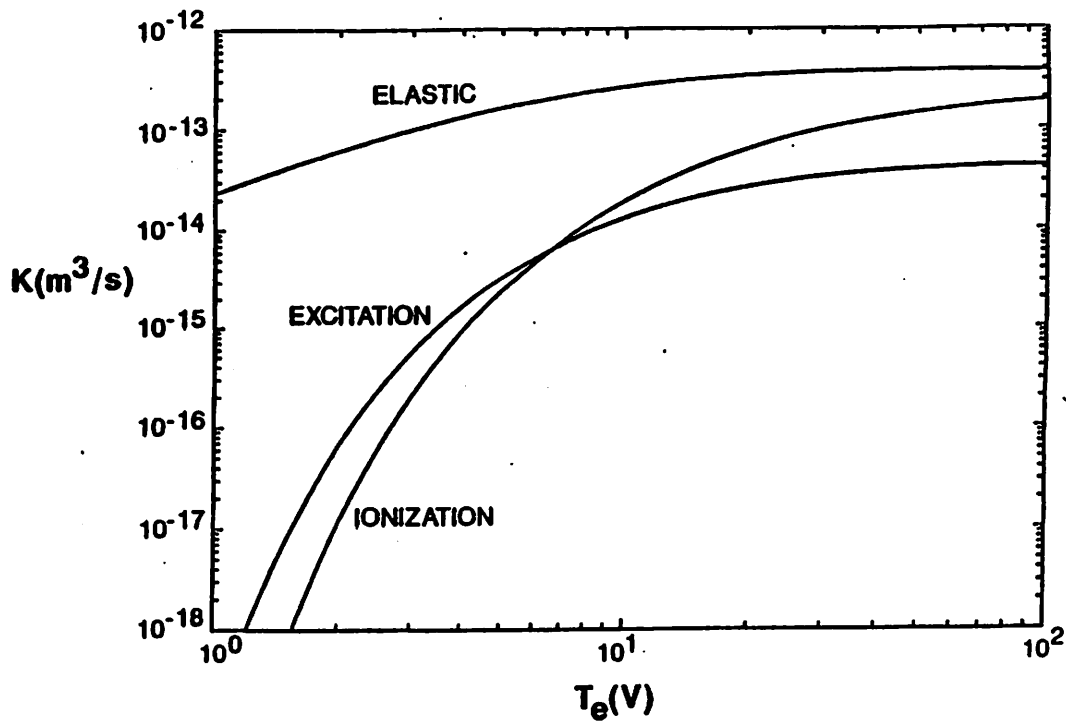


Figure 6: Electron neutral collision rate coefficients for momentum transfer, ionization and excitation as a function of electron temperature in argon gas (From M.A. Lieberman and R.A. Gottscho, in *Physics of Thin Films*, vol. 18, edited by M. Francombe and J. Vossen, Academic Press, 1994).

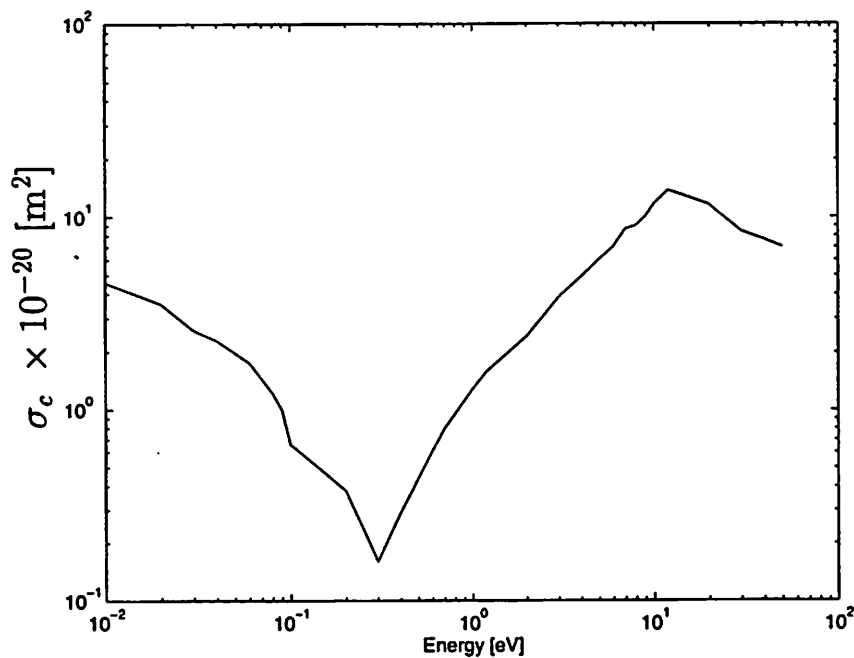


Figure 7: The total cross section for electron-momentum transfer σ_c for argon.

3.4.2 Stochastic Interaction

Piejak et al. [2] have measured the effect of collisionless heating in inductive discharges. Turner [15] and Vahedi et al. [14] have shown that collisionless heating is important for low pressure operation where nonlocal effects are important. If the electron transit time through the power absorption region is shorter than the rf period then the electron is nonadiabatically heated and there is a net energy gain. Vahedi et al. [14] define a stochastic (collisionless) frequency ν_{st} by equating the collisionless power, at low pressure where almost all the energy is deposited in the electrons through collisionless mechanism, to an effective collisional heating power. They define

$$\alpha_T = \frac{4\delta^2\omega^2}{\pi\bar{v}_e^2} = \left(\frac{\text{Transit time of a thermal electron through skin depth}}{\text{rf period}} \right)^2 \quad (48)$$

and for the case where the applied frequency is roughly equal to the transit frequency of the electron ($\alpha_T \sim 1$) they obtain $\nu_{st}/\omega \leq 1$. In this limit the stochastic collision frequency is approximated by

$$\nu_{st} \approx \frac{1}{4} \frac{\bar{v}_e}{\delta} \quad (49)$$

where $\bar{v}_e = (8kT_e/\pi m)^{1/2}$ is the mean speed of the electrons.

3.4.3 Coulomb Interactions

At very high density the electron-ion collision frequency is expected to have an effect on the effective electron collision frequency. Miyamoto [16, p. 96] gives the electron-electron collision frequency as

$$\nu_{ee} = \frac{n_e e^4 \ln \Lambda}{2\pi \epsilon_0^2 m^2 \bar{v}_e^3} \quad (50)$$

and the electron-ion collision frequency as $\nu_{ei} = \frac{1}{2}\nu_{ee}$ where $\ln \Lambda$ is the Coulomb logarithm given as [17]

$$\ln \Lambda = 23 - \ln \left[\frac{n_e^{1/2} T_e^{-3/2}}{10^2} \right] \quad (51)$$

for $T_e \leq 10$ V and n_e is in the units of m^{-3} .

3.5 Skin Depth

In an inductively coupled plasma discharge, the power is transferred from the electric fields to the plasma within a skin depth layer of thickness δ next to the quartz window by either a collision dissipation or stochastic process. In the typical operating range of inductive discharges, $p = 1 - 100$ mTorr, we find $\nu_{eff} \leq \omega$.

The plasma skin depth is related to the plasma electron density by [14]

$$\delta = \frac{c}{\omega_{pe}} \left(\frac{2 \left(1 + \frac{\nu_{eff}^2}{\omega^2} \right)}{\beta \left(1 + \left(1 + \frac{\nu_{eff}^2}{\omega^2 \beta^2} \right)^{1/2} \right)} \right)^{1/2} \quad (52)$$

where

$$\beta = 1 + \alpha \left(1 + \nu_{eff}^2 / \omega^2 \right) \quad (53)$$

and

$$\alpha = \left(\frac{c}{\omega_{pe}} \right)^2 \left[\left(\frac{3.83}{R} \right)^2 - \left(\frac{\omega}{c} \right)^2 \right] \quad (54)$$

are geometrical correction factors and ν_{eff} is the effective collision frequency as defined by equation (41). Solving equation (52) for the plasma frequency ω_{pe} gives

$$\omega_{pe} = \left(\frac{e^2 n_{av}}{\epsilon_0 m} \right)^{1/2} \quad (55)$$

where n_{av} is the average electron density in the power absorption region.

3.5.1 Collisional Limit

In the collisional limit $\nu_{eff} \gg \omega$ the skin depth can be approximated by

$$\delta = \frac{c}{\omega_{pe}} \left(\frac{2\nu_{eff}}{\omega} \right)^{1/2} \quad (56)$$

so the the plasma resistance R_2 , in terms of the skin depth, becomes

$$R_2 = 3.80 \times \frac{\omega \delta}{c^2 \epsilon_0} \quad (57)$$

In this approximation the electron-ion collision frequency is

$$\nu_{ei} = \frac{c^2 e^2 \nu_{eff} \ln \Lambda}{2\pi \omega \epsilon_0 m \delta^2 \bar{v}_e^3} \quad (58)$$

and

$$\ln \Lambda = 23 - \ln \left[\frac{c T_e^{3/2} (2\nu_{eff})^{1/2}}{e \delta \omega^{1/2}} \left(\frac{\epsilon_0 m_e}{10^4} \right)^{1/2} \right] \quad (59)$$

The effective collision frequency is calculated by solving equation (41) for ν_{eff} .

3.5.2 Collisionless Limit

In the collisionless limit $\nu_{eff} \ll \omega$ the effective resistance remains non-zero when collisional effects are ignorable so

$$R_2 = 3.80 \times \frac{\nu_{eff} \delta}{c^2 \epsilon_o} \quad (60)$$

and the skin depth is approximated by

$$\delta = \frac{c}{\omega_{pe}} \quad (61)$$

Applying this approximation for the skin depth the electron-ion collision frequency becomes

$$\nu_{ei} = \frac{c^2 e^2 \ln \Lambda}{4\pi \epsilon_o m \delta^2 \bar{v}_e^3} \quad (62)$$

and the Coulomb logarithm

$$\ln \Lambda = 23 - \ln \left[\frac{c T_e^{3/2}}{e \delta} \left(\frac{\epsilon_o m_e}{10^4} \right)^{1/2} \right] \quad (63)$$

The effective collision frequency is calculated as before using equation (41).

4 Density Profile and Sheath Edge Density

The power absorption takes place at the axial sheath edge of the plasma where the electron density is lower than at the center of the bulk plasma. In low pressure discharges, assuming that the ion drift velocity due to the ambipolar electric field dominates the diffusion, a differential equation describing the density profile can be derived (see e.g. [18, p. 137]). In one-dimensional planar geometry this is

$$u_B \left(\frac{2\lambda_i}{\pi} \right)^{1/2} \frac{d}{dx} \left(-n \frac{dn}{dx} \right)^{1/2} = \nu_{iz} n \quad (64)$$

where $u_B = (kT_e/m_i)^{1/2}$ is the Bohm velocity and ν_{iz} is the ionization collision frequency. This differential equation is nonlinear and has been solved by Godyak and Maximov [19, 20] for $u_i = u_B$ at the sheath edge. They give the solution for the density $n(\delta)$ at the power absorption region $z = \delta$ as

$$\theta^{2/3} \chi = \frac{1}{2} \ln \left[(1 - h^3)^{1/3} + h \right] + \frac{1}{\sqrt{3}} \arctan \left[\frac{2(h^{-3} - 1)^{1/3} - 1}{\sqrt{3}} \right] + \frac{\pi}{6\sqrt{3}} \quad (65)$$

where $\chi = 2(\frac{1}{2}L - \delta)/L$, $h = n(\delta)/n_o$ and

$$\theta = \frac{\nu_{iz} L}{2u_B} \left(\frac{\pi L}{4\lambda_i} \right)^{1/2} \approx 1.25 \quad (66)$$

where n_o is the electron density at the center of the bulk plasma,

$$\lambda_i = \frac{1}{n_g \sigma_i} \quad (67)$$

is the ion neutral mean free path, $\sigma_i \approx 10^{-18} \text{ m}^2$ is the ion-atom scattering cross section for low energy ions [18, p. 80],

$$\nu_{iz} = K_{iz} n_g \quad (68)$$

is the ionization frequency, and K_{iz} is the ionization rate constant. A similar solution can be given for one-dimensional cylindrical geometry. Godyak and Maximov [19, 20] give an approximate equation for the axial sheath edge density, where the drift velocity is equal to the Bohm velocity, as

$$h_L \equiv \frac{n_s L}{n_o} \approx \frac{0.86}{\sqrt{\left(3 + \frac{L}{2\lambda_i}\right)}} \quad (69)$$

and for the radial sheath edge density

$$h_R \equiv \frac{n_s R}{n_o} \approx \frac{0.80}{\sqrt{\left(4 + \frac{R}{\lambda_i}\right)}} \quad (70)$$

Solving equation (65) for the normalized electron density one skin depth away from the quartz window $h(\delta)$ we can relate the average density in the power absorption region to the center density

$$n_{av} \approx \frac{h_L + h(\delta)}{2} n_o \quad (71)$$

or

$$n_o \approx \frac{2n_{av}}{h_L + h(\delta)} \quad (72)$$

and the electron density at the sheath edge is

$$n_{sL} \equiv h_L n_o \approx \frac{2n_{av} h_L}{h_L + h(\delta)} \quad (73)$$

5 Power Balance

The electron density is related to the power absorbed within the plasma via the overall discharge power balance. The overall discharge power balance for a cylindrical plasma having radius R and length L is written as [18, p. 304]

$$P_{abs} = en_s u_B A \mathcal{E}_T \quad (74)$$

where P_{abs} is the power absorbed within the plasma, n_s is the ion density at the sheath edge, A is the area for particle loss, and \mathcal{E}_T is the total energy lost per ion lost from the system

$$\mathcal{E}_T = \mathcal{E}_c + \mathcal{E}_e + \mathcal{E}_i \quad (75)$$

where \mathcal{E}_c is the collisional energy lost per electron-ion pair created, $\mathcal{E}_e \approx 2T_e$ is the mean kinetic energy lost per electron lost, and \mathcal{E}_i is the mean kinetic energy lost per ion lost and is the sum of the ion energy entering the sheath and the energy gained by the ion as it traverses the sheath.

Equation (74) can be written as

$$n_o = \frac{P_{abs}}{eu_B A_{eff} \mathcal{E}_T} \quad (76)$$

where n_o is the center (bulk) electron density and the effective area A_{eff} is defined to account for possibly different values of the density at the radial and axial sheath edge as

$$A_{eff} = 2\pi R(Rh_L + Lh_R) \quad (77)$$

such that $n_s A = n_o A_{eff}$. For a specified density and electron temperature the absorbed power can be determined. The electron temperature can be determined by equating the total volume ionization to the surface particle loss to obtain [5]

$$\frac{K_{iz}}{u_B} = \frac{1}{n_g d_{eff}} \quad (78)$$

where

$$d_{eff} = \frac{1}{2} \frac{RL}{Rh_L + Lh_R} \quad (79)$$

is an effective plasma size and K_{iz} is the rate constant for electron-neutral ionization. Equation (78) thus determines the electron temperature for a given gas pressure.

For argon $\mathcal{E}_i \approx 5.2T_e$ and \mathcal{E}_c can be estimated from figure 8 (from [5]). \mathcal{E}_c accounts for the loss of electron energy due to ionization, excitation and elastic scattering against neutral atoms.

A crude analytical approximation to K_{iz} in a limited range of electron temperature is [18, p. 80]

$$K_{iz} \approx K_{izo} \exp(-\mathcal{E}_{iz}/T_e) \quad (80)$$

where for argon $\mathcal{E}_{iz} \approx 15.76$ V is the ionization energy and $K_{izo} \approx 5 \times 10^{-14}$ m³/s. Solving equation (78) using equation (80) for argon gives an estimate of the electron temperature for different values of gas pressure.

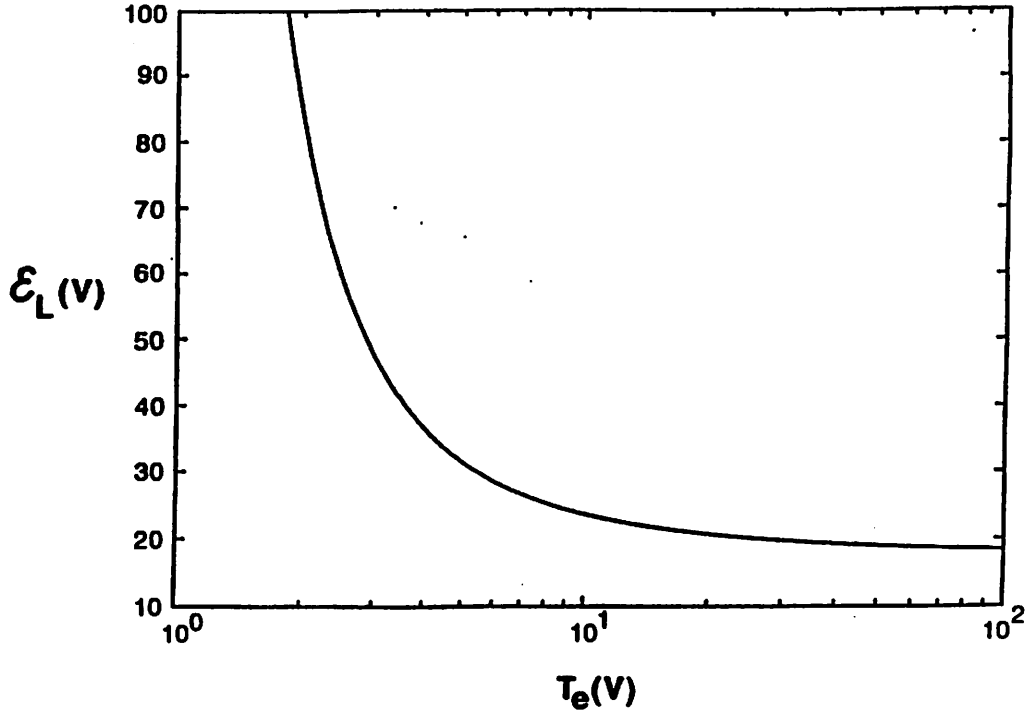


Figure 8: Collisional energy loss per electron-ion pair created \mathcal{E}_c as a function of electron temperature T_e in argon gas (From M.A. Lieberman and R.A. Gottscho, in *Physics of Thin Films*, vol. 18, edited by M. Francombe and J. Vossen, Academic Press, 1994).

6 Experimental Results

This preceding simple model is applied to the discharge described in section 2 for argon plasma at pressures of 2, 10, 20 and 60 mTorr. The neutral gas temperature T_g is assumed to be 473 K. This assumption overestimates the temperature and thus underestimates slightly the electron neutral collision frequency at high absorbed power but overestimates the temperature at low absorbed power. The driving frequency used is $\omega/2\pi = 13.56$ MHz. The electron energy distribution function used in equation (46) is considered to be Maxwellian

$$f(\mathcal{E}) = \frac{2}{\sqrt{\pi}} \frac{1}{(eT_e)^{3/2}} \exp\left(-\frac{\mathcal{E}}{T_e}\right) \quad (81)$$

where T_e is the electron temperature. The relation between the plasma skin depth and the average electron density in the power absorption region is determined using equations (52) – (55) and is plotted in figure 9. The skin depth depends on the electron density of the plasma, the electron temperature, the neutral gas pressure and temperature through the electron neutral collision frequency and the electron temperature through the stochastic collision frequency. The electron density is calculated by solving equation (52) for a given skin depth, electron temperature, neutral gas pressure and the neutral gas temperature. The typical operating range for inductive

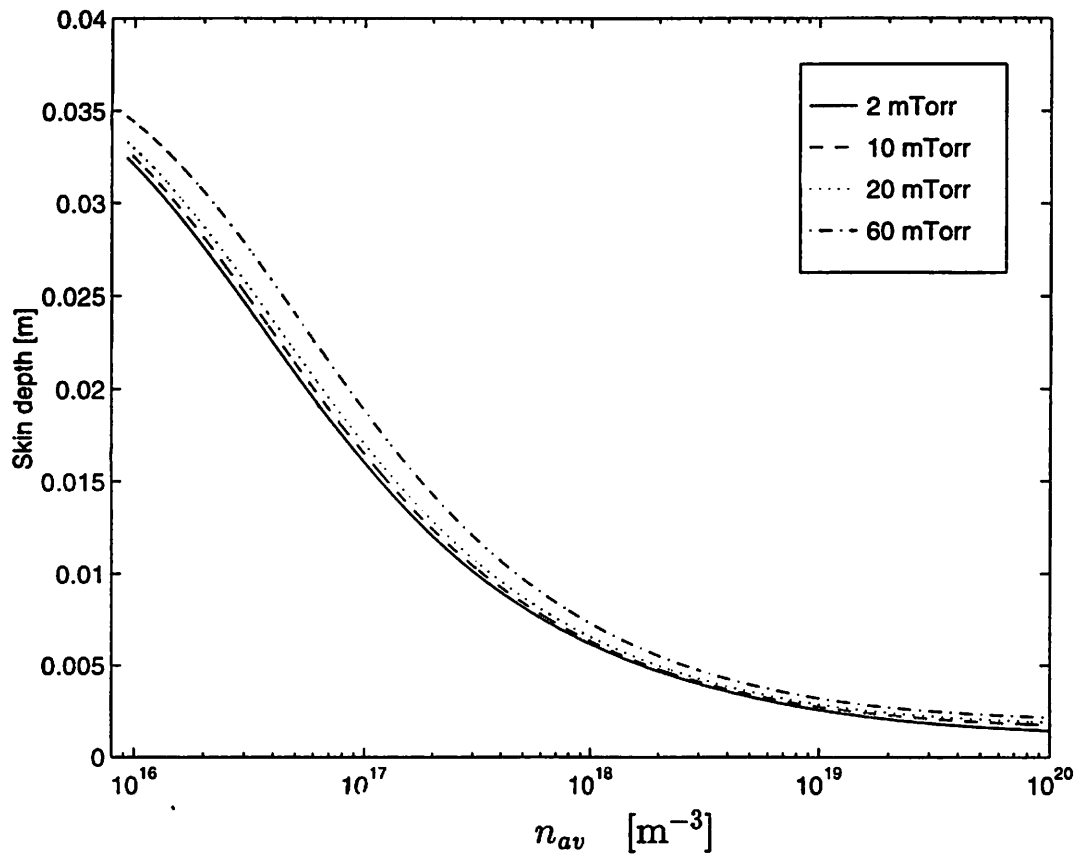


Figure 9: The plasma skin depth versus the average density in the power absorption region of the plasma for argon plasma at — 2 mTorr, - - 10 mTorr \cdots 20 mTorr and - . - 60 mTorr.

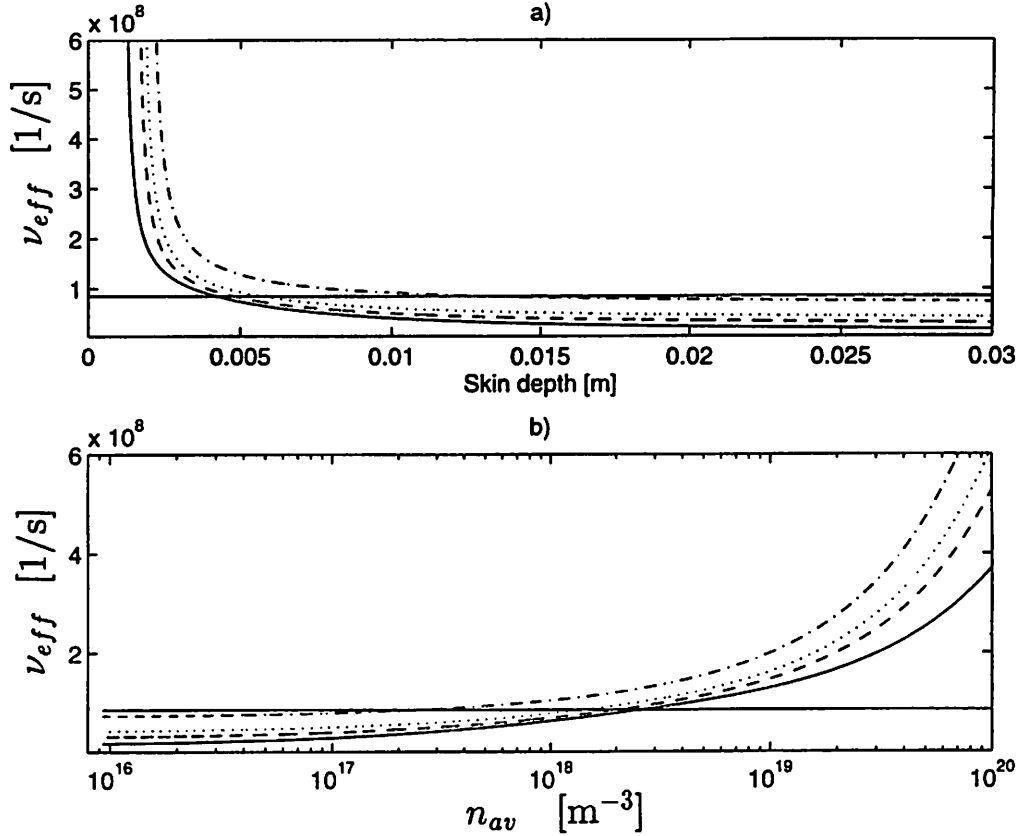


Figure 10: The effective collision frequency ν_{eff} (a) versus the skin depth of the plasma δ , (b) versus the average density in the power absorption region for argon plasma at — 2 mTorr, - - 10 mTorr \cdots 20 mTorr and - · - 60 mTorr. The solid horizontal line represents the driving frequency ω .

discharges corresponds to an average density in the power absorption region, n_{av} , in the range $10^{16} - 10^{18} \text{ m}^{-3}$ and to a skin depth of 1 – 3 cm. There is a weak dependence on neutral gas pressure due to the pressure dependence of the collision frequency. The approximation used for the stochastic collision frequency, $\nu_{st} \approx \frac{1}{4} \bar{v}_e / \delta$ is valid only for $0.03 \leq \alpha_T \leq 10$ [14]. Calculations show that α_T is within this range except for very high densities. This approximation is valid for densities up to $n_{av} \approx 10^{20} \text{ m}^{-3}$. The effective collision frequency is the sum of electron neutral collision frequency, the stochastic collision frequency and electron-ion collision frequency, and its dependence on skin depth and electron density is shown in figures 10 (a) and 10 (b) respectively. The effective collision frequency peaks at low skin depth (high density), is of the order of the driving frequency over most of the range of interest but falls off with skin depth due to the stochastic term $\nu_{st} \propto \bar{v}_e / \delta$. The values of electron temperature used to

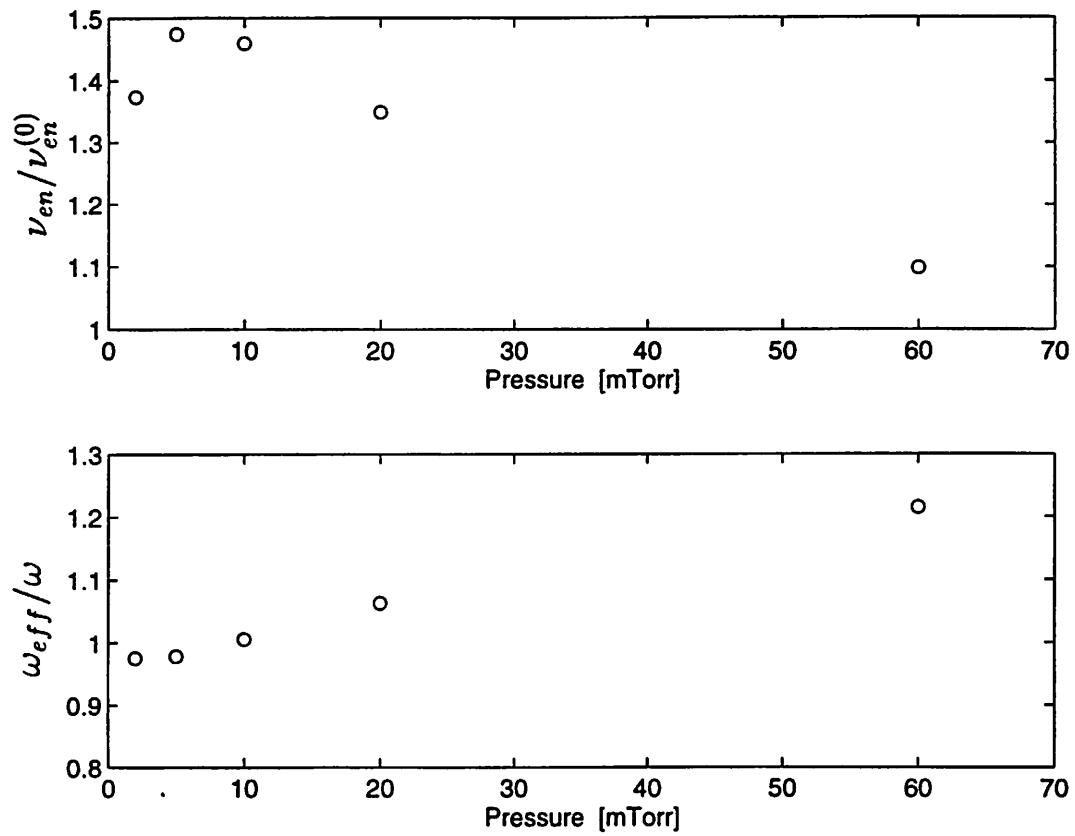


Figure 11: (a) The ratio $\nu_{en}/\nu_{en}^{(0)}$ versus the neutral gas pressure. (b) The ratio ω_{eff}/ω versus the neutral gas pressure for argon plasma.

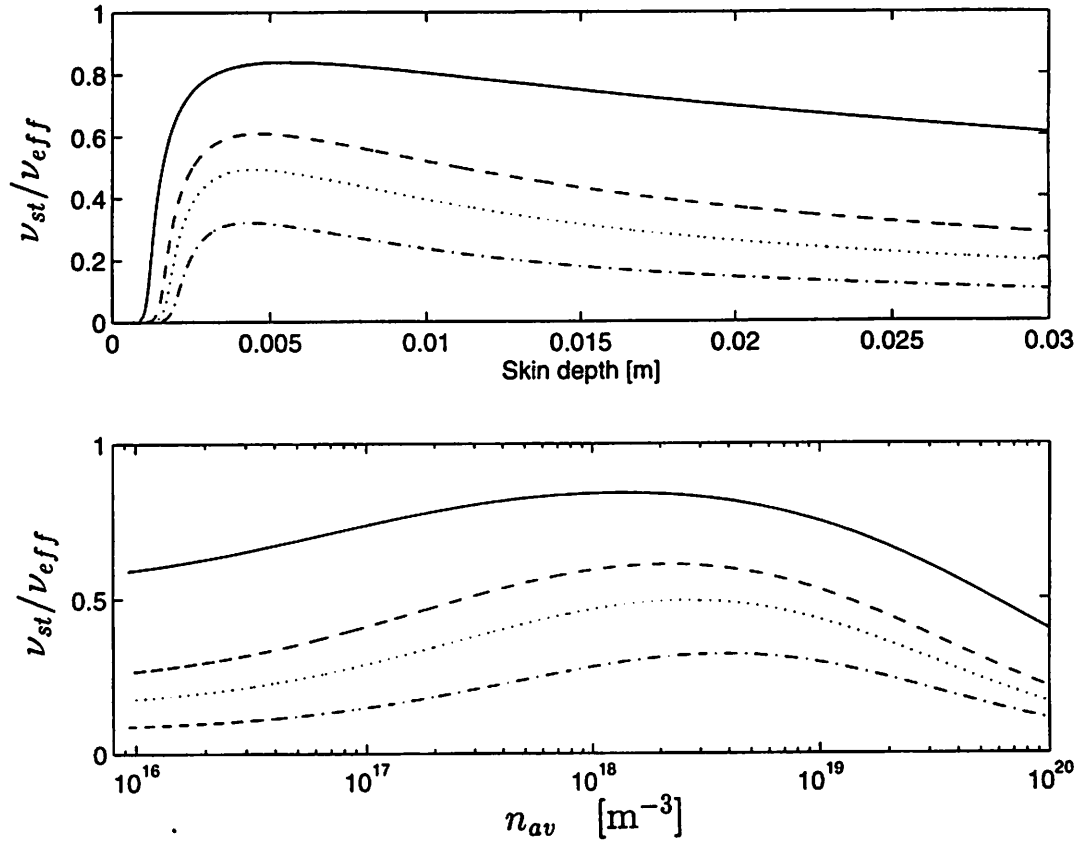


Figure 12: The ratio of the stochastic collision frequency ν_{st} to the effective collision frequency ν_{eff} (a) versus the skin depth the plasma δ , (b) versus the average density in the power absorption region for argon plasma at — 2 mTorr, - - 10 mTorr, \cdots 20 mTorr and - . - 60 mTorr.

evaluate the stochastic collision frequency are calculated by solving equation (78). In figure 11 (a) the ratio $\nu_{en}/\nu_{en}^{(o)}$ is plotted versus the neutral gas pressure and in figure 11 (b) the ratio ω_{eff}/ω is plotted versus the neutral gas pressure. Figure 12 shows the ratio of the stochastic collision frequency over the effective collision frequency, ν_{st}/ν_{eff} . We note that the stochastic collision frequency becomes the dominant collision frequency and thus the dominant heating mechanism at low pressure. Even at higher pressure stochastic heating plays an important role in the overall heating mechanism. The effect of the electron-ion collision frequency on the heating mechanism is shown in figure 13 where the electron-ion collision frequency over the effective collision frequency is plotted versus the skin depth (a) and average electron density in the power absorption region. As expected this heating mechanism is relatively most effective at high electron density and more so at higher neutral gas pressure due to the $T_e^{-3/2}$ dependence of ν_{ei} .

7 Transformer Model

In this simple model the mutual inductance between the two coils as well as the geometrical inductance of the current loop formed within the plasma, the secondary coil, only depend on the skin depth of the plasma. The mutual inductance between the two coils is seen in figure 14 (a) as a function of the skin depth of the plasma. The solid line shows the mutual inductance calculated according to Lyle's method as described in section 3.1.3 and the dashed line shows the result using the simple approach described in section 3.1.1. As expected using the simple approach underestimates the mutual inductance. Figure 14 (b) shows the mutual inductance (Lyle's method) versus the average electron density n_{av} in the power absorption region next to the quartz window.

The self inductance of the secondary coil is shown as a function of the skin depth in figure 15 (a). The self inductance is calculated using equation (31). The pressure dependence of the self inductance when viewed as a function of the skin depth is due to the loop expansion parameter γ . The self inductance of the secondary coil versus density is shown in figure 15 (b) for several different values of pressure. There is additional pressure dependence when the self inductance is viewed as a function of the electron density due to the pressure dependence of the effective electron collision frequency. The approximation, equation (33) overestimates the self inductance and this overestimate increases as the skin depth increases. This is reasonable since this approximation assumes $\kappa \approx 1$ or κ' small, which is valid only if δ is small.

The plasma resistance is calculated using equation (39) and is shown versus skin

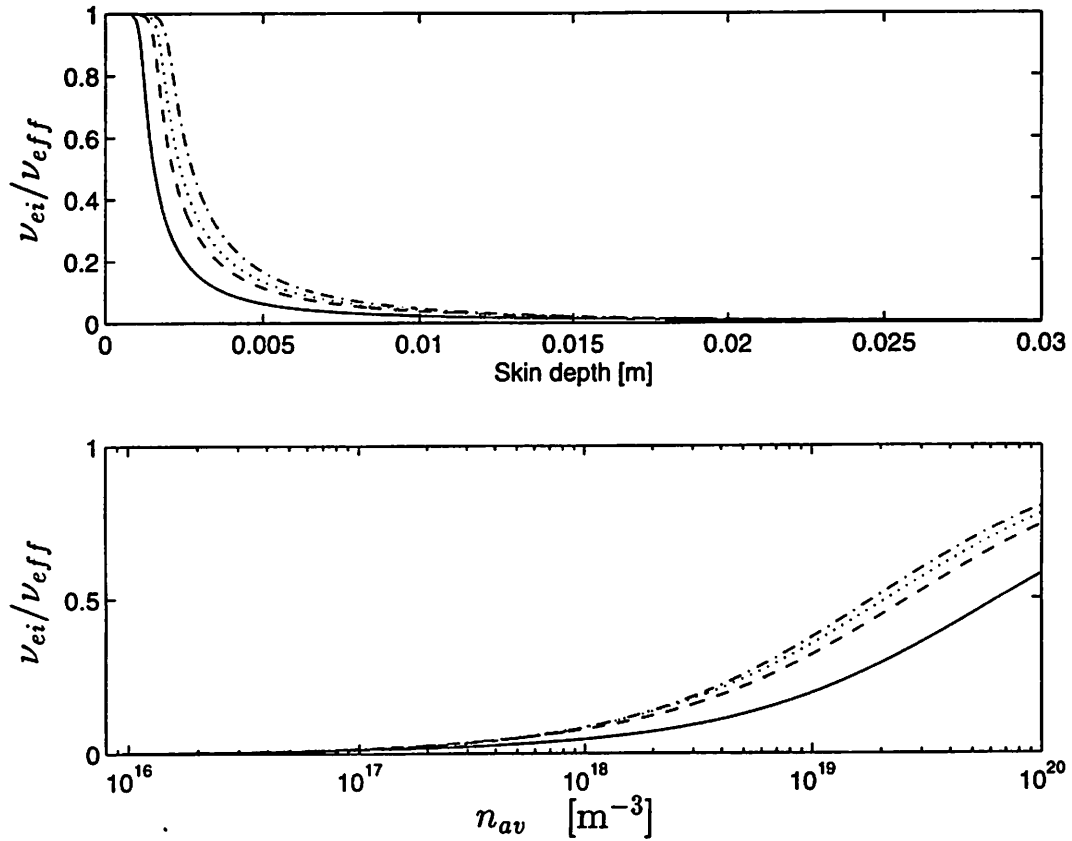


Figure 13: The ratio of the electron-ion collision frequency ν_{ei} to the effective collision frequency ν_{eff} (a) versus the skin depth of the plasma δ , (b) versus the average density in the power absorption region for argon plasma at — 2 mTorr, - - 10 mTorr \cdots 20 mTorr and - · - 60 mTorr.

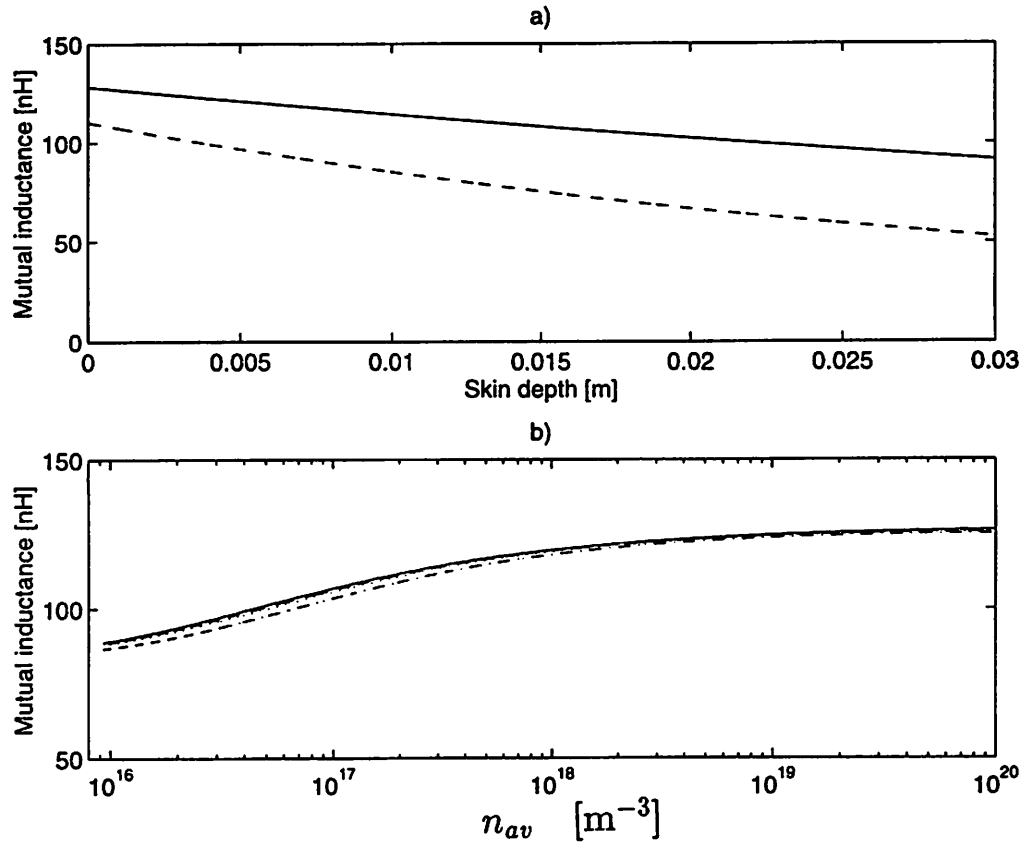


Figure 14: (a) The mutual inductance M versus the skin depth of the plasma. The solid line shows the mutual inductance calculated applying Lyle's method and the dashed line shows the mutual inductance calculated according to the simple approach. b) The mutual inductance M calculated by Lyle's method versus the average density in the power absorption region of the plasma for argon plasma at — 2 mTorr, - - 10 mTorr \cdots 20 mTorr and - \cdot - 60 mTorr.

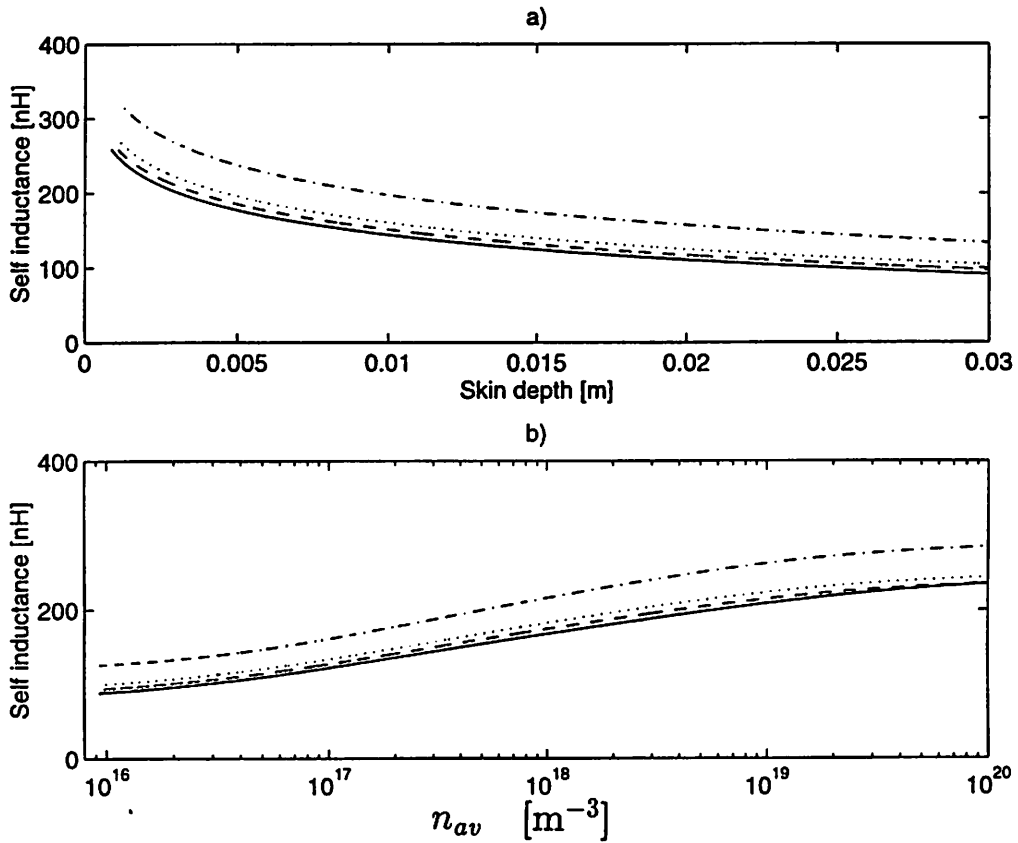


Figure 15: The geometrical self inductance of the conducting path in the plasma, L_2 , (a) versus the skin depth of the plasma δ , (b) versus the average density in the power absorption region for argon plasma at — 2 mTorr, - - 10 mTorr \cdots 20 mTorr and - \cdot - 60 mTorr.

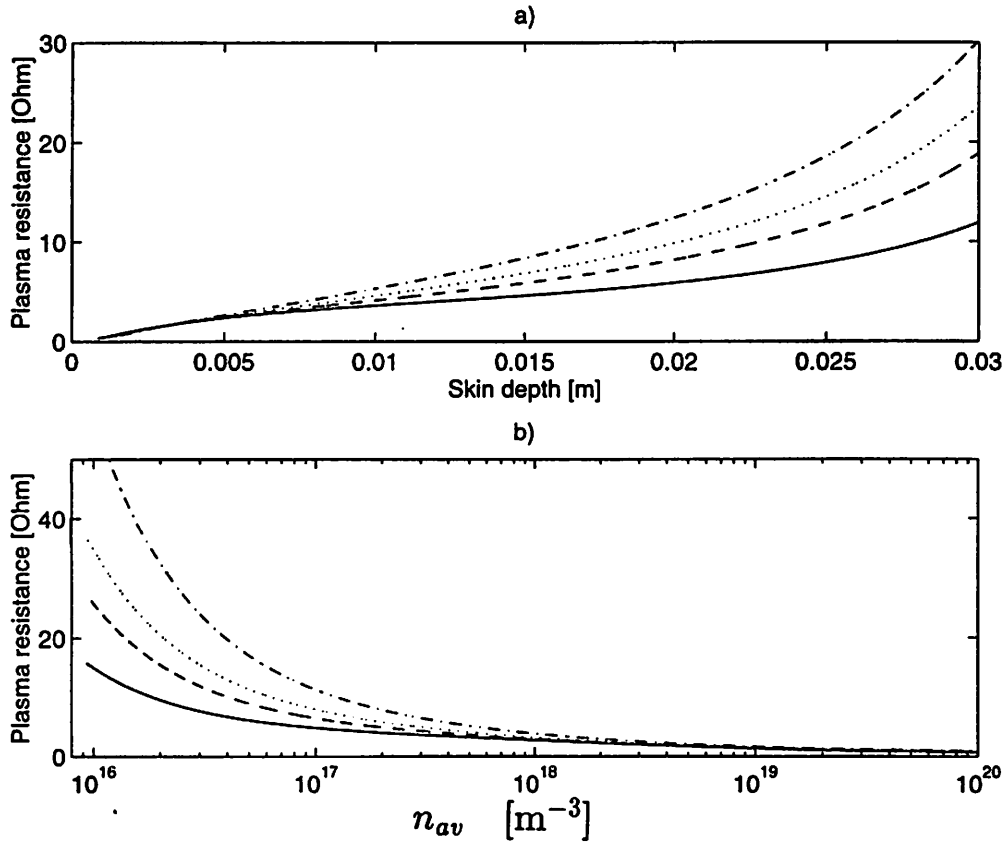


Figure 16: The resistance of the conducting path in the plasma, R_2 , (a) versus the skin depth of the plasma δ , (b) versus the average density in the power absorption region for argon plasma at — 2 mTorr, - - 10 mTorr \cdots 20 mTorr and - \cdot - 60 mTorr.

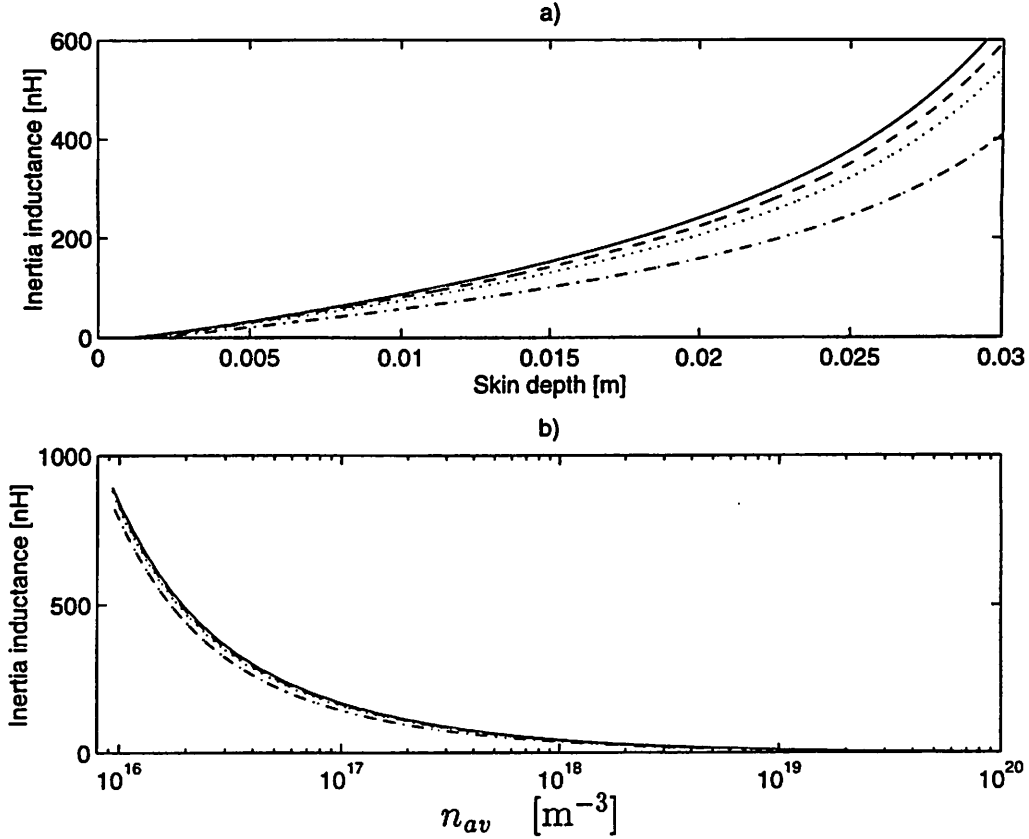


Figure 17: The electron inertia inductance in the plasma L_e (a) versus the skin depth of the plasma δ , (b) versus the average density in the power absorption region for argon plasma at — 2 mTorr, - - 10 mTorr \cdots 20 mTorr and - \cdot - 60 mTorr.

depth and average electron density n_{av} in figures 16 (a) and 16 (b) respectively. At very high densities (small skin depth) the plasma resistance approaches zero, but increases as the density falls. The highest density region corresponds to a transformer with the secondary circuit shorted; the resistance R_2 approaches zero. In the lowest density region the resistance goes up rapidly and the circuit properties approach that of an open secondary circuit. The electron inertia inductance shown in figures 17 (a) and 17 (b) shows similar behavior.

The calculated values M , L_2 , R_2 , and L_e are used in equation (40) to give the change in resistance seen in the primary circuit ρ as a function of the skin depth and electron density. This is seen in figures 18 (a) and 18 (b). This resistance is seen to increase with skin depth to a maximum value and then fall approximately off as $\propto 1/\delta$ as the skin depth is increased further. In figures 19 (a) - 19 (d) this behavior is investigated further. The theoretical value of ρ calculated using equation (52) is

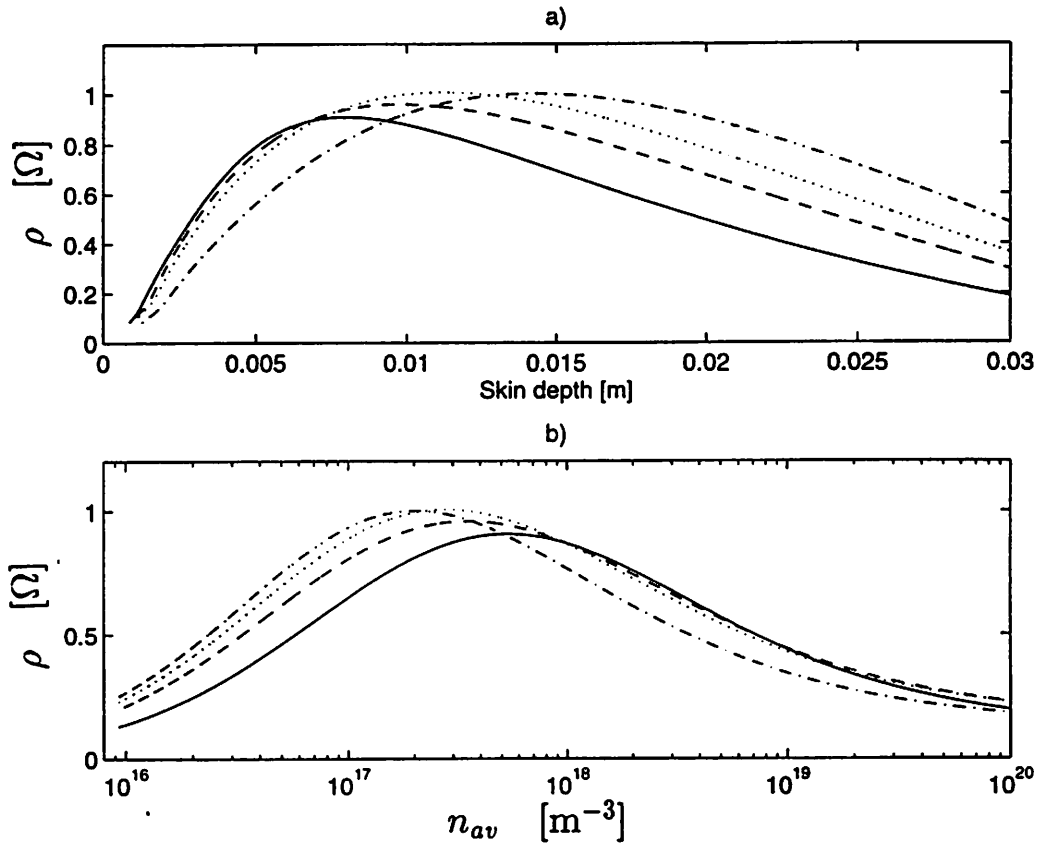


Figure 18: The changes in primary resistance due to plasma loading, ρ , (a) versus the skin depth of the plasma, δ , (b) versus the average density in the power absorption region for argon plasma at — 2 mTorr, - - 10 mTorr \cdots 20 mTorr and - · - 60 mTorr.

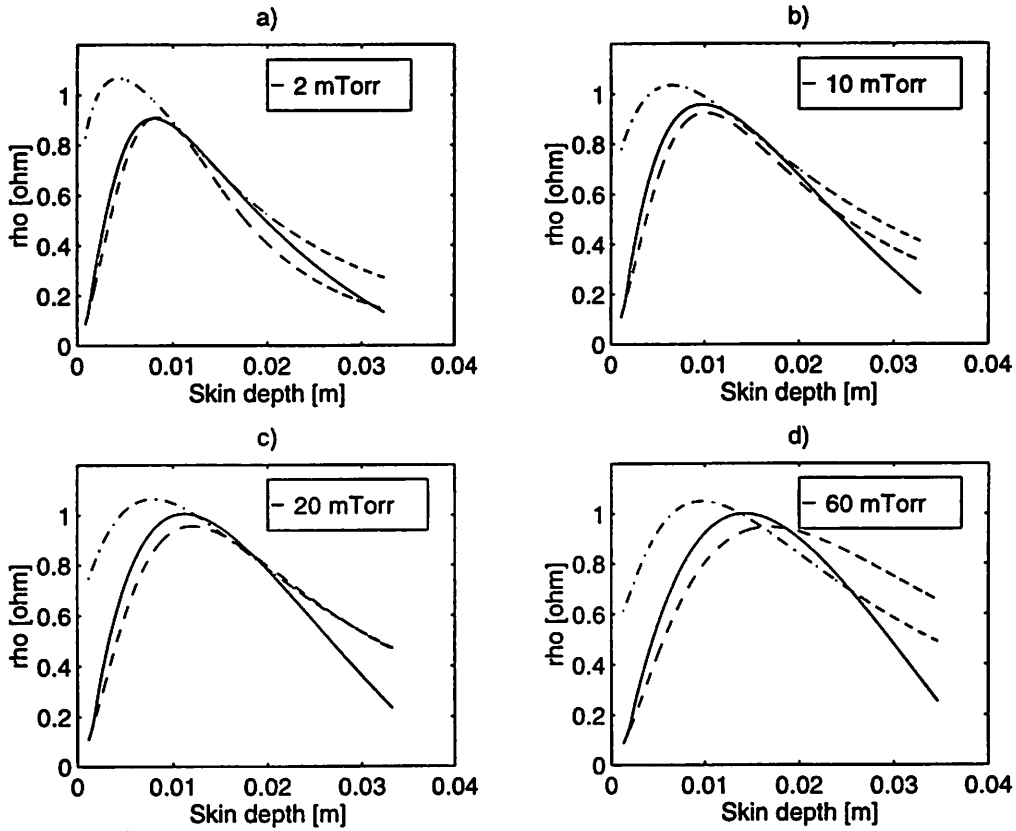


Figure 19: The changes in primary resistance due to plasma loading, ρ , (solid line) versus the skin depth of the plasma, δ , compared to the collisionless $- \cdot -$ and collisional $--$ limit (a) at 2 mTorr argon pressure, (b) at 10 mTorr argon pressure, (c) at 20 mTorr argon pressure and (d) at 60 mTorr argon pressure.

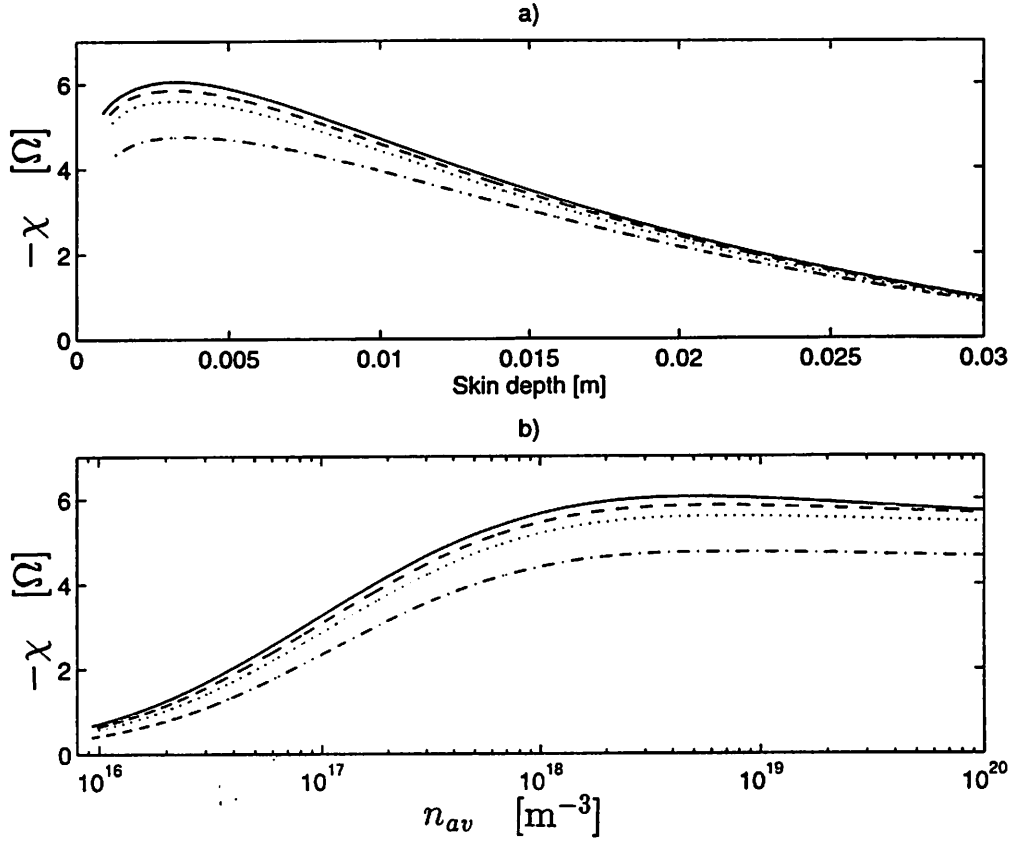


Figure 20: The negative of the change in primary reactance due to plasma loading, $-\chi$ (a), versus the skin depth of the plasma δ , (b) versus the average density in the power absorption region for argon plasma at — 2 mTorr, - - 10 mTorr \cdots 20 mTorr and - · - 60 mTorr.

compared to the value calculated using the collisional and collisionless approximations for the skin depth. At the smallest skin depth (highest density) the collisionless approximation is not valid. In this range the collisional approximation underestimates the resistance change. As the pressure is increased and electron density decreases, the approximations become more inaccurate. Figure 20 (a) shows the negative of the change in primary reactance, $-\chi$, due to the plasma load versus the skin depth and figure 20 (b) shows $-\chi$ versus average electron density n_{av} in the power absorption region.

7.1 Argon Plasma

The resistance due to plasma loading as seen in the primary circuit is plotted as a function of the power absorbed within the plasma in figure 21, where the calculated value is compared to measured values for argon plasma in the pressure range 2 – 60 mTorr. The power absorbed in the plasma is determined by measuring the power incident when plasma is present in the source and the current is applied and subtracting the power incident when no plasma is present at the same applied current:

$$P_{abs} |_{I_{rf}} = P_{inc}(\text{plasma}) - P_{inc}(\text{no plasma}) |_{I_{rf}} \quad (82)$$

The power and the current were measured when no plasma is present to give the resistance of the primary coil R_o and with plasma present to give the resistance R_1 . The resistance due to the plasma load is then

$$\rho = R_1 - R_o \quad (83)$$

The model gives a reasonable estimate of the resistance change due to the plasma loading at both low and high pressures. This model underestimates the resistance change slightly which may be due to capacitive power transfer in the discharge. Note that there is no electrostatic shield between the coil and the plasma so some degree of capacitive power transfer is expected. This may explain the discrepancy between the model and the measured data.

Figure 22 shows the negative of the change in reactance as seen in the primary circuit due to plasma loading versus power absorbed within the plasma. The rf voltage across the coil is measured with and without plasma and the inductance is found from solving

$$|V_{rf}| = [(\omega L_o + \chi)^2 + (R_o + \rho)^2]^{1/2} |I_{rf}| \quad (84)$$

for the reactance change

$$\chi = \left[\left(\frac{|V_{rf}|}{|I_{rf}|} \right)^2 - \left(\frac{P_{inc}}{|I_{rf}|^2} \right)^2 \right]^{1/2} - \omega L_o \quad (85)$$

where P_{inc} is the input power when V_{rf} is applied across the primary coil and the current I_{rf} is flowing through the primary coil. At low power there is a discrepancy between the simple model and the measured data. This may be due to capacitive effects in the power coupling which is expected at low power, but not accounted for in this simple model. At higher power where the power coupling can be expected to

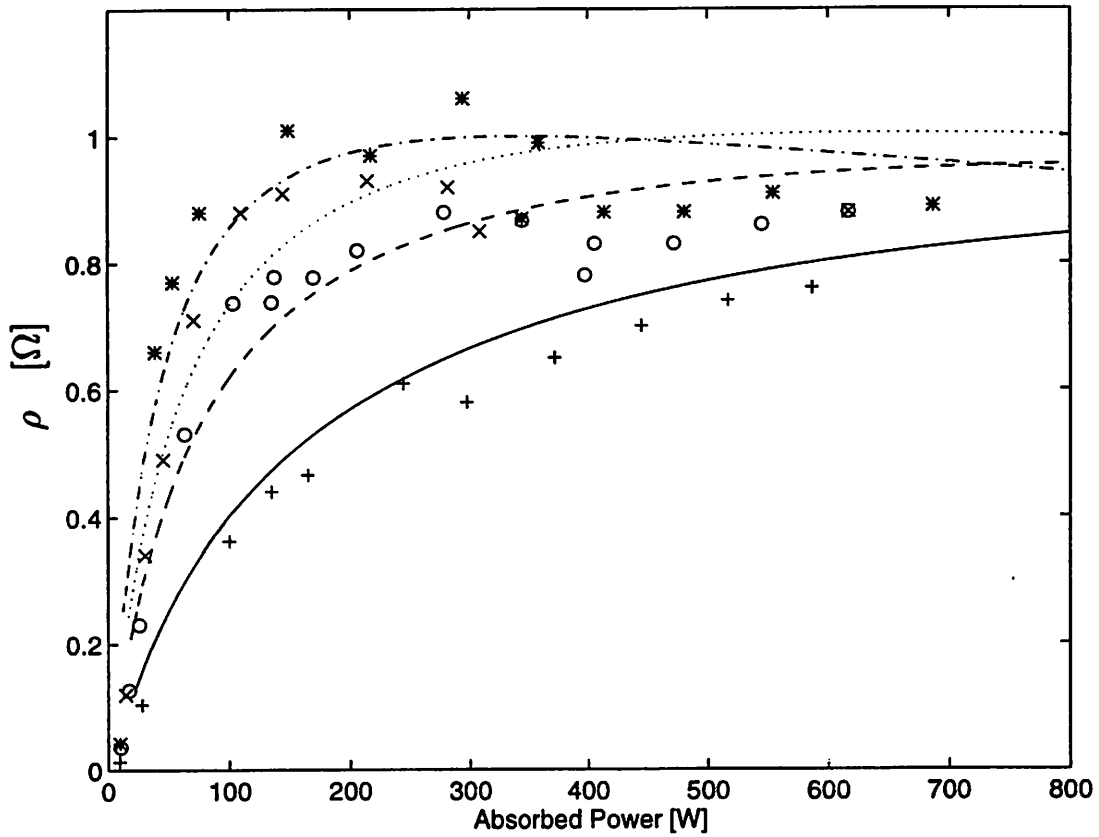


Figure 21: The changes in primary resistance due to plasma loading, ρ , versus the power absorbed within the plasma for argon plasma at — 2 mTorr, - - 10 mTorr \cdots 20 mTorr and - · - 60 mTorr compared to measured resistance for argon plasma at + 2 mTorr, o 10 mTorr, x 20 mTorr and * 60 mTorr.

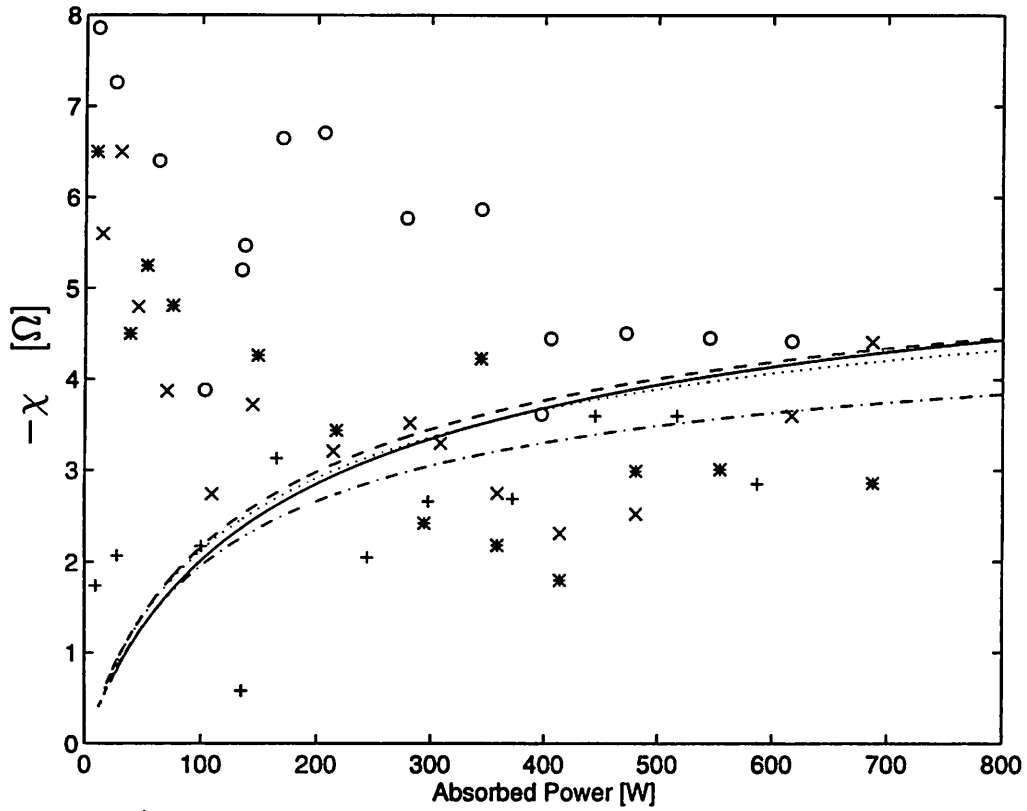


Figure 22: The negative of the change in primary reactance due to plasma loading, $-\chi$, versus the power absorbed within the plasma for argon plasma at — 2 mTorr, - - 10 mTorr \cdots 20 mTorr and - · - 60 mTorr compared to measured reactance for argon plasma at + 2 mTorr, o 10 mTorr, \times 20 mTorr and * 60 mTorr.

be purely inductive, the correlation between the model and the measured reactance is reasonable.

With decreasing neutral gas pressure, a higher rf current is required to sustain the discharge. This is seen in figure 23, where the simple model calculations are compared to measured rf current values for argon plasma. Higher current results in lower power transfer efficiency since $P_{loss} = I_{rf}^2 R_o$ where R_o is the resistance of the matching circuit and the coil in the absence of plasma. Larger rf current also results in higher coil voltage V_{rf} , since $V_{rf} = I_{rf} |Z_s|$ where Z_s is given by equation (9). This is seen in figure 24 where the model calculations are compared to measured data for argon plasmas in the pressure range 2 - 60 mTorr. To apply equation (9) to calculate Z_s , the inductance of the primary inductive coil, L_o , is needed. In the absence of plasma assuming $V_{rf} \approx |\omega L_o| I_{rf}$ we measured the average value $L_o \approx 482.6$ nH. The coil inductance L_o measured in the absence of plasma decreases slightly as the power to the coil is increased. This explains some of the deviation of the measured rf voltage data (symbols) from the model calculations (curves), that use the average value of L_o , at higher power.

7.2 Ar versus SF₆ and O₂ plasma

The changes in the primary coil resistance due to plasma loading at 10 mTorr pressure are shown in figure 25. The model calculations for argon plasma are compared to the measured resistance for Ar, O₂, SF₆ and 25%Ar/75%SF₆ plasma. The oxygen plasma requires higher power than argon plasma to reach the plateau, which is believed to indicate purely inductive coupling. SF₆ requires the highest power to reach that plateau resistance value. Ar, O₂ and SF₆ are measured to have roughly the same resistance in purely inductive mode. Figure 26 shows the negative of the reactance change as seen in the primary loop due to plasma loading versus the absorbed power. The calculated reactance change is compared to measured values for Ar, O₂, SF₆ and 25%Ar/75%SF₆ plasma at 10 mTorr. The measured reactance change decreases with increased electronegativity of the gas.

8 Conclusion

A simple model assuming purely inductive coupling between a planar inductive coil and a discharge plasma in argon is described. The mutual inductance between the inductive coil and the plasma, the self inductance created in the plasma, the plasma resistance and the inertia inductance are calculated from first principles and are given

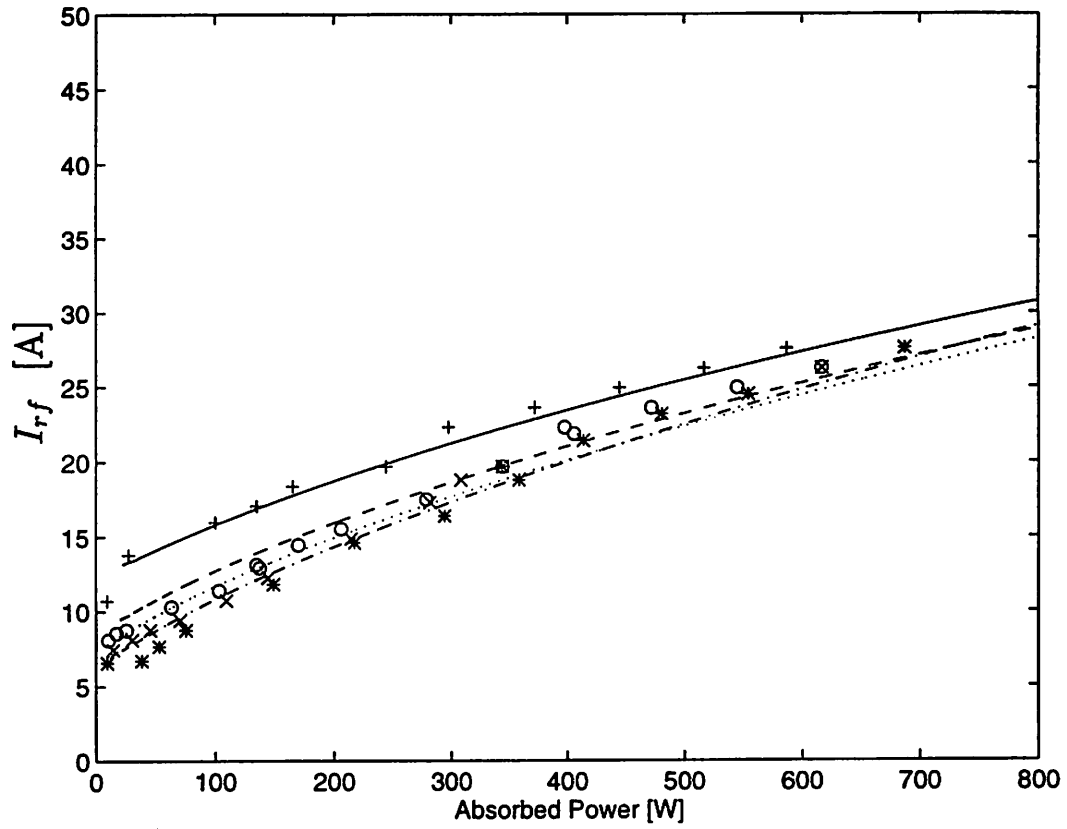


Figure 23: The rf current I_{rf} applied to the primary coil versus the power absorbed within the plasma for argon plasma at — 2 mTorr, - - 10 mTorr \cdots 20 mTorr and - · - 60 mTorr compared to measured rf current applied to discharge for argon plasma at + 2 mTorr, o 10 mTorr, x 20 mTorr and * 60 mTorr.

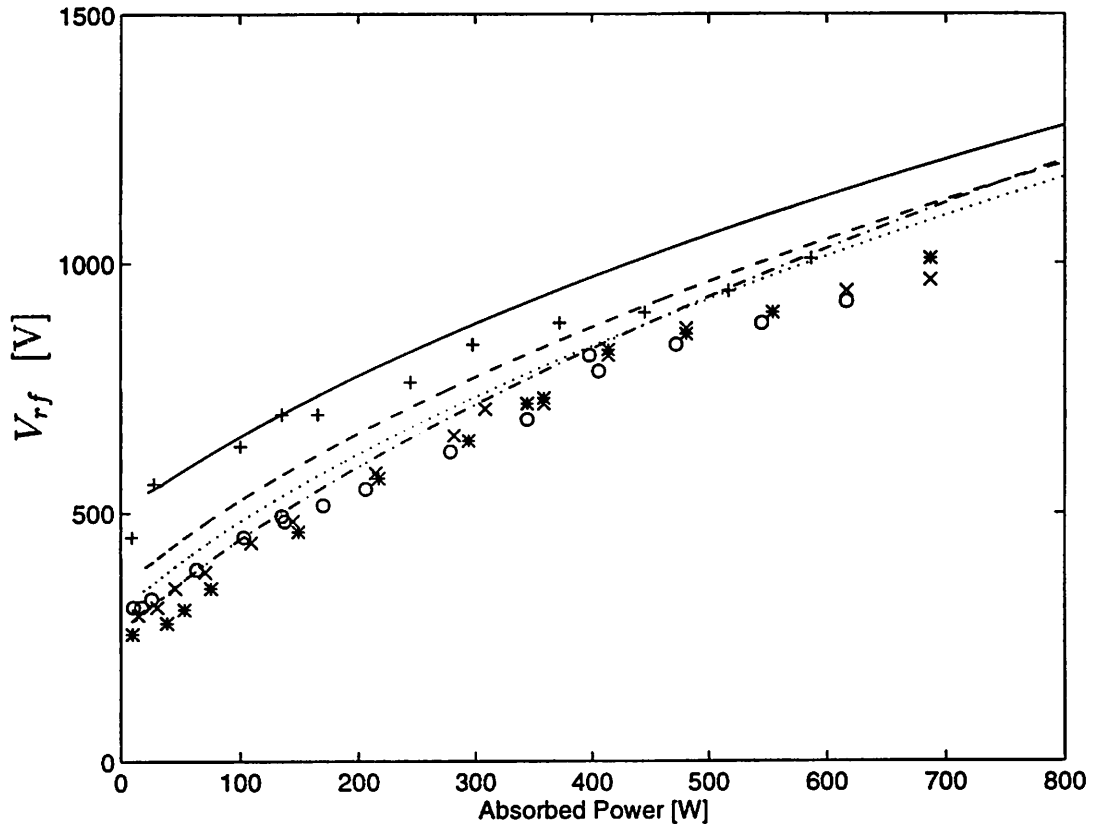


Figure 24: The rf voltage V_{rf} applied to the primary coil versus the power absorbed within the plasma for argon plasma at — 2 mTorr, - - 10 mTorr \cdots 20 mTorr and - · - 60 mTorr compared to measured rf voltage applied to discharge for argon plasma at + 2 mTorr, o 10 mTorr, x 20 mTorr and * 60 mTorr.

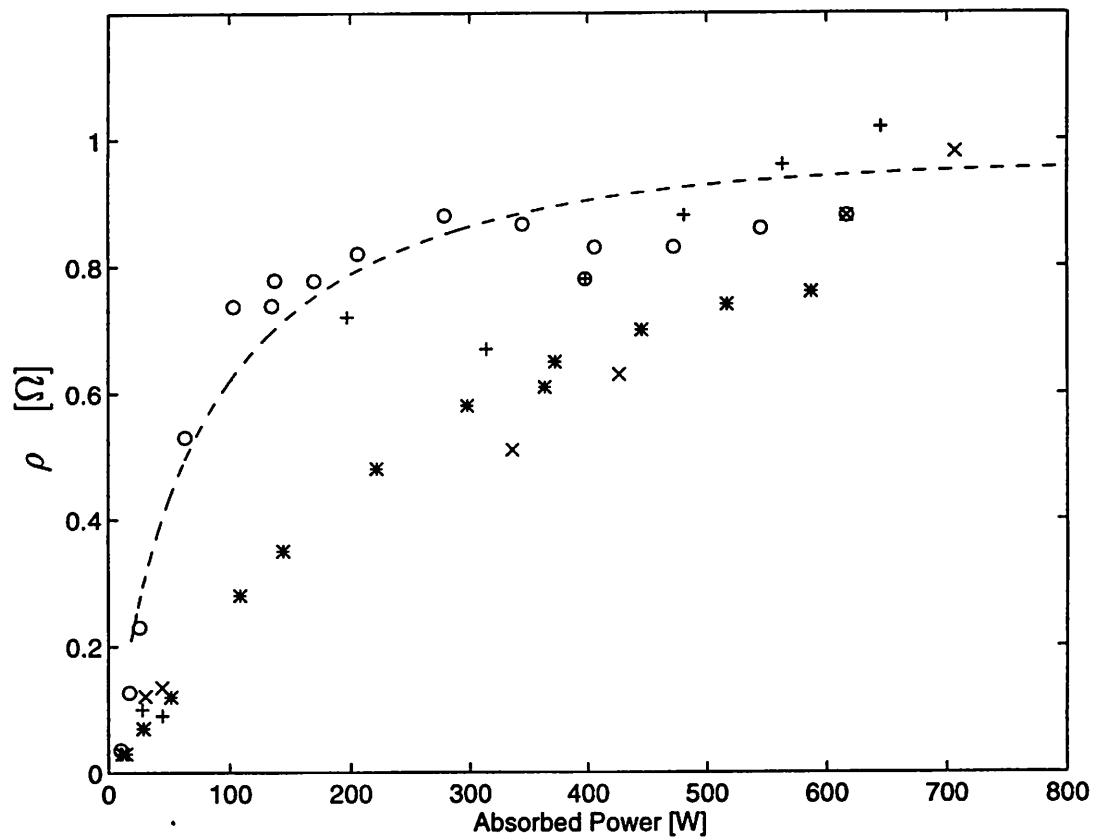


Figure 25: The changes in primary resistance due to plasma loading, ρ , versus the power absorbed within the plasma for \circ Ar, $*$ O_2 , $+$ 25%Ar/75%SF₆ and \times SF₆ plasma at 10 mTorr compared to the calculated value for argon plasma.

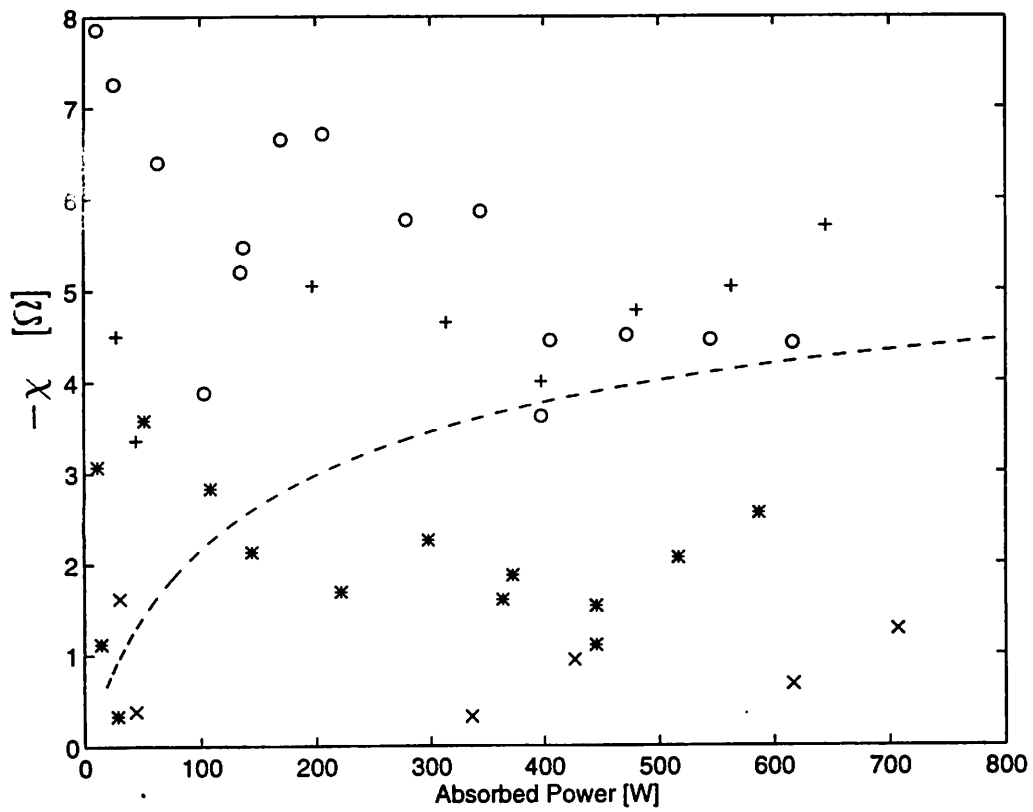


Figure 26: The negative of the change in primary reactance due to plasma loading, $-\chi$, versus the power absorbed within the plasma for \circ Ar, $*$ O₂, $+$ 25%Ar/75%SF₆ and \times SF₆ plasma at 10 mTorr compared to the calculated value for argon plasma.

as a function of the skin depth of the plasma and the plasma electron density for argon plasma. These circuit elements are used, modeling the discharge as a transformer, to calculate the impedance characteristics of the plasma as seen in the transformer primary circuit. The impedance change due to plasma loading is compared to the measured impedance change in argon plasma. The model gives a good estimate of the real part of the impedance, the resistance change, but there is a discrepancy in the imaginary part, the reactance change, at low power and pressure. This discrepancy may be due to capacitive effects in the power coupling, expected at low power and pressure, that are not included in this model. Comparison of the argon model to measurements in electronegative gases indicates that the discrepancy in the reactance values increases as the electronegativity increases. When in purely inductive mode the model can be used to estimate the electrical characteristics of a discharge and the rf voltage and rf current required to sustain the discharge can be predicted. Further work is underway to incorporate capacitive power transfer and negative ions into the model.

The authors would like to thank D. Baca for experimental assistance. This work was partially supported by LLNL/PPRI Grant B291464, Lam Research Corporation, NSF Grant ECS-9217500, and DOE Grant DE-FG03-87ER13727.

References

- [1] J. Tykocinski-Tykociner, *Philosophical Magazine* **13** (1932) 953 - 963
- [2] R.B. Piejak, V.A. Godyak and B.M. Alexandrovich, *Plasma Sources Science and Technology* **1** (1992) 179 - 186
- [3] V.A. Godyak, R.B. Piejak and B.M. Alexandrovich, *Plasma Sources Science and Technology* **3** (1994) 169 - 176
- [4] G.G. Lister, Y-M Li and V.A. Godyak, submitted to *Journal of Applied Physics*(1995)
- [5] M.A. Lieberman and R.A. Gottscho, in *Physics of Thin Films*, vol. 18, edited by M. Francombe and J. Vossen, Academic Press, 1994
- [6] J.C. Maxwell, *Treatise on Electricity and Magnetism*, Clarendon Press, 1891
- [7] R.K. Wangsness, *Electromagnetic Fields*, John Wiley & Sons, 1979

- [8] H.L. Curtis and C.M. Sparks, *Scientific Papers of the Bureau of Standards* **19** (1924) 541 - 576
- [9] T.R. Lyle, *Philosophical Magazine* **3** (1902) 310 - 329
- [10] F.W. Grover, *Inductance Calculations: Working Formulas and Tables*, D. Van Nostrand, 1946
- [11] J. Hopwood, C.R. Guarnieri, S.J. Whitehair and J.J. Cuomo, *Journal of Vacuum Science and Technology A* **11** (1993) 147 - 151
- [12] J.A. Meyer and A.E. Wendt, *Journal of Applied Physics* **78** (1995) 90 - 96
- [13] S. Ramo, J.R. Whinnery and T. Van Duzer, *Fields and Waves in Communication Electronics*, John Wiley & Sons, 1967
- [14] V. Vahedi, M.A. Lieberman, G. Dipeso, T.D. Rognlien and D. Hewett, *Journal of Applied Physics* **78** (1995) 1446 - 1458
- [15] M.M. Turner, *Physical Review Letters* **71** (1993) 1844 - 1847
- [16] K. Miyamoto, *Plasma Physics for Nuclear Fusion*, The MIT Press, 1989
- [17] D.L. Book, *NRL Plasma Formulary*, Naval Research Laboratory, 1990
- [18] M.A. Lieberman and A.J. Lichtenberg, *Principles of Plasma Discharges and Materials Processing*, John Wiley & Sons, 1994
- [19] V.A. Godyak and V.N. Maximov, *Vestnik Moskovskogo Universiteta, ser. Physica i Astronomia* **18** (1977) 51 - 56
- [20] V.A. Godyak, *Soviet Radio Requency Discharge Research*, Delphic Associates, Falls Churc V.A., 1986

Symbol Definitions

a_i	mean radius of the i th turn of the primary coil [m]
A	area [m ²]
A_{eff}	effective area [m ²]
b	mean radius of the plasma disk [m]
d	distance between the center planes of the circular loops [m]
d_{eff}	effective plasma length [m]
\mathcal{E}_c	collisional energy lost per electron-ion pair created [V]
\mathcal{E}_e	kinetic energy lost per electron lost [V]

\mathcal{E}_i	kinetic energy lost per ion lost [V]
\mathcal{E}_{iz}	ionization energy [V]
h	dimensionless density
h_L	density center to edge ratio
I	current [A]
I_e	electron current [A]
I_{rf}	rms current in the primary loop [A]
K_{el}	momentum transfer rate constant [m ³ /s]
K_{iz}	ionization rate constant [m ³ /s]
L	inductance [H], length of vacuum chamber [m]
L_o	inductance of primary loop [H]
L_1	inductance of primary loop under plasma load [H]
L_2	geometrical inductance of plasma loop [H]
L_e	inductance due to electron inertia in plasma [H]
L_s	inductance seen in the primary loop [H]
m	electron mass [kg]
m_i	ion mass [kg]
M	mutual inductance [H]
n	density [m ⁻³]
n_{av}	average electron density in the power absorption region [m ⁻³]
n_e	electron density [m ⁻³]
n_g	neutral gas density [m ⁻³]
n_i	ion density [m ⁻³]
P_{abs}	power absorbed by plasma [W]
P_2	power dissipated in the secondary circuit [W]
r_1	parameter defined by equation (17)
r_2	parameter defined by equation (18)
R	radius of the vacuum chamber [m]
R_o	resistance of the primary coil [Ω]
R_1	resistance of the primary coil under plasma load [Ω]
R_2	resistance of the plasma loop [Ω]
T_e	electron temperature [V]
T_g	neutral gas temperature [K]
u_B	Bohm velocity [m/s]
w_q	thickness of quartz plate [m]
Z_2	impedance of plasma loop [Ω]
α	geometrical parameter in equation (54)

α_T	ratio of the transit time of an electron through skin depth to rf period squared
β	geometrical parameter defined in equation (53)
χ	changes in primary reactance due to plasma load [Ω]
δ	skin depth [m]
Δ	separation of primary coil from quartz window [m]
ζ_1	half the equivalent depth of the primary coil [m]
ζ_2	half the equivalent depth of the plasma loop [m]
η_1	axial depth of inductive coil [m]
η_2	axial depth of plasma loop [m]
κ	parameter defined by equation (13)
κ'	parameter defined by equation (14)
λ_i	ion neutral mean free path [m]
Λ	parameter defined in equation (51)
ν	collision frequency [1/s]
ν_{eff}	effective collision frequency [1/s]
ν_{ee}	electron-electron collision frequency [1/s]
ν_{ei}	electron-ion collision frequency [1/s]
ν_{en}	electron-neutral collision frequency [1/s]
ν_{st}	stochastic collision frequency [1/s]
ξ_1	axial breadth of inductive coil [m]
ξ_2	axial breadth of plasma loop [m]
φ	magnetic flux [$T \cdot m^2$]
ρ	changes in primary resistance due to plasma load [Ω]
ϱ	equivalent radius of plasma loop [m]
σ_c	total cross section for electron-momentum transfer [m^2]
σ_p	electrical plasma conductance [$1 / \Omega m$]
θ	parameter defined by equation (66)
ω	angular driving frequency [rad/s]
ω_{eff}	effective angular driving frequency [rad/s]
ω_p	angular plasma frequency [rad/s]